ANTIOXIDANTS & REDOX SIGNALING
Volume 30, Number 16, 2019

DOI: 10.1089/ars.2018.7545

Discoveries

ORIGINAL RESEARCH COMMUNICATION

Transient Receptor Potential Canonical 3 and Nuclear Factor of Activated T Cells C3 Signaling Pathway Critically Regulates Myocardial Fibrosis

Youakim Saliba,[1] Victor Jebara,[2,*] Joelle Hajal,[1,*] Richard Maroun,[3] Stéphanie Chacar,[1,3] Viviane Smayra,[2] Joel Abramowitz,[4] Lutz Birnbaumer,[4,5] and Nassim Farès[1]

Abstract

Aims: Cardiac fibroblasts (CFs) are emerging as major contributors to myocardial fibrosis (MF), a final common pathway of many etiologies of heart disease. Here, we studied the functional relevance of transient receptor potential canonical 3 (TRPC3) channels and nuclear factor of activated T cells c3 (NFATc3) signaling in rodent and human ventricular CFs, and whether their modulation would limit MF.

Results: A positive feedback loop between TRPC3 and NFATc3 drove a rat ventricular CF fibrotic phenotype. In these cells, polyphenols (extract of grape pomace polyphenol [P.E.]) decreased basal and angiotensin II-mediated Ca^{2+} entries through a direct modulation of TRPC3 channels and subsequently NFATc3 signaling, abrogating myofibroblast differentiation, fibrosis and inflammation, as well as an oxidative stress-associated phenotype. N(ω)-nitro-L-arginine methyl ester (L-NAME) hypertensive rats developed coronary perivascular, sub-epicardial, and interstitial fibrosis with induction of embryonic epicardial progenitor transcription factors in activated CFs. P.E. treatment reduced ventricular CF activation by modulating the TRPC3-NFATc3 pathway, and it ameliorated echocardiographic parameters, cardiac stress markers, and MF in L-NAME hypertensive rats independently of blood pressure regulation. Further, genetic deletion ($TRPC3^{-/-}$) and pharmacological channel blockade with N-[4-[3,5-Bis(trifluoromethyl)-1H-pyrazol-1-yl]phenyl]-4-methyl-benzenesulfonamide (Pyr10) blunted ventricular CF activation and MF in L-NAME hypertensive mice. Finally, TRPC3 was present in human ventricular CFs and upregulated in MF, whereas pharmacological modulation of TRPC3-NFATc3 decreased proliferation and collagen secretion.

Innovation and Conclusion: We demonstrate that TRPC3-NFATc3 signaling is modulated by P.E. and critically regulates ventricular CF phenotype and MF. These findings strongly argue for P.E., through TRPC3 targeting, as potential and interesting therapeutics for MF management. *Antioxid. Redox Signal.* 30, 1851–1879.

Keywords: myocardial fibrosis, ventricular cardiac fibroblasts, TRPC3/NFATc3, polyphenols, calcium, cardiac fibroblast progenitors

[1]Laboratoire de Recherche en Physiologie et Physiopathologie, Pôle Technologie Santé, Faculté de Médecine, Université Saint Joseph, Beirut, Lebanon.
[2]Faculté de Médecine, Université Saint Joseph, Beirut, Lebanon.
[3]Unité de Recherche Technologie et Valorisation Alimentaire, Centre d'Analyses et de Recherche, Faculté des Sciences, Université Saint-Joseph, Beirut, Lebanon.
[4]Neurobiology Laboratory, National Institute of Environmental Health Sciences, Durham, North Carolina.
[5]Institute of Biomedical Research (BIOMED), School of Medicine, Catholic University of Argentina, Buenos Aires, Argentina.
*Both these authors contributed equally to this work.

Innovation

We provide the first evidence that functional transient receptor potential canonical 3 (TRPC3) is present in human ventricular cardiac fibroblasts (CFs) and is associated with myocardial fibrosis (MF). Modulation of TRPC3 channels and nuclear factor of activated T cells c3 (NFATc3) signaling by polyphenols in human and rodent ventricular CFs abrogates their fibrotic phenotype. Pharmacological and genetic inhibition of TRPC3 ameliorates hypertension-induced MF by decreasing CF activation in a blood pressure-independent way. These findings strongly argue for polyphenols, through their TRPC3 targeting, as potential and interesting myocardial anti-fibrotic therapeutics.

Introduction

A common feature of all etiologies of heart disease is excessive deposition of extracellular matrix (ECM) by cardiac fibroblasts (CFs), leading to myocardial fibrosis (MF). CF is emerging as a significant yet understudied major contributor of this disease, emphasizing the biological importance of MF and its compelling candidacy as a potential therapeutic target (61, 65).

On acute injury or chronic sustained stress on the myocardium, CFs transdifferentiate into myofibroblasts with a pronounced secretory profile for the ECM components, leading to MF (7, 28, 47). Myofibroblasts also arise from a number of potentially different cell sources within the injured heart, although the exact origin remains controversial. Epithelial-to-mesenchymal transition (73), endothelial-to-mesenchymal transition (72), pericytes (26), bone marrow-derived myeloid cells (67), and other infiltrating immune cells (17) have been all proposed as origins.

Several other studies have challenged these findings and demonstrated that resident fibroblasts of epicardial origin, expressing among other progenitor transcription factors, transcription factor 21 (TCF21), platelet-derived growth factor receptor alpha (PDGFRα), and Wilms tumor 1 (Wt1), give rise to myofibroblasts in the hypertrophied and failing heart (20, 35, 36, 50). Therefore, elaborating a clear picture of CF lineage development and accumulation in the injured heart would be essential for developing anti-fibrotic therapies. The purpose of all this adaptive response is to maintain the structural integrity of the heart; however, this process becomes detrimental in the long run, leading to the progression into heart failure.

Transient receptor potential canonical (TRPC) channels have been described in ventricular CFs. A non-selective cation current likely carried by TRPCs was present in rat CF and angiotensin II (AngII) stimulated nuclear factor of activated T cells c3 (NFATc3) signaling (14, 49). Though TRPC6-NFAT signaling has been shown as a molecular circuit for myofibroblast transformation and tissue repair (6), the same pathway has been intriguingly described as an inhibitor of CF transdifferentiation (37). Transient receptor potential canonical 3 (TRPC3) and TRPC6 are closely homologous channels belonging to the receptor-operated channels activated by diacylglycerol (DAG). Finally, TRPC3 has been described as a pro-fibrotic channel in neonatal ventricular fibroblasts and TRPC3 deletion inhibited maladaptive fibrosis in pressure-overloaded mouse hearts (39, 40). However, data on ventricular CFs from adult rodent hearts and most importantly the role of TRPC3-NFAT in human ventricular CF physiology and its relevance to human MF remain largely unknown.

Dietary polyphenols have been shown to promote cardiovascular health and limit the progression to disease (41, 48, 63). Interestingly, these compounds also displayed intracellular Ca^{2+} signaling modulatory effects on several cell types, which suggested properties beyond their anti-oxidant capacities (10). However, the main concern that hindered the translation of such results in humans is the use in practically all of the studies of non-physiological concentrations of polyphenols in cell cultures, and *in vivo* doses that are impractical in humans. In addition to that is the low bioavailability of polyphenols due to their excessive metabolism in the body (15). This spurred into many controversies on the potential benefits of polyphenols and whether these compounds could be useful to humans (45, 69).

Despite the conflicting data, encouraging epidemiological and interventional studies are still emerging on the beneficial role of dietary polyphenols in affecting vascular function and improving cardiovascular risk (2, 33, 38, 66). Precisely, polyphenol-rich diets have shown more consistent results in cardiovascular disease prevention with synergistic interactions leading to improved efficacy (12) as compared with single compound consumptions or supplementations (51, 60).

In this study, we checked whether direct modulation of TRPC3 channels and NFATc3 signaling *in vitro* in rat ventricular CFs by polyphenols as well as specific channel pharmacological inhibition would abrogate the fibrotic phenotype of ventricular CFs. We then tested the hypothesis that modulating TRPC3-NFATc3 *in vivo* in ventricular CFs either by polyphenols in N(ω)-nitro-L-arginine methyl ester (L-NAME) hypertensive rats or by specific pharmacological inhibition and genetic deletion ($TRPC3^{-/-}$) in L-NAME hypertensive mice would diminish MF in a blood pressure-independent way. The purpose was to evaluate the impact of a combination of phenolic compounds reflecting a feasible daily consumption of these products as a mixture in a matrix of food. Low concentrations were used *in vitro*, reflecting their bioavailability in human parallel-to-low *in vivo* doses with analogy to a well-balanced polyphenol-rich diet. Finally, we evaluated the functional relevance of TRPC3-NFATc3 signaling in human ventricular CFs, its association to MF and modulation by polyphenols.

Results

TRPC3 modulation by extract of grape pomace polyphenol suppresses myofibroblast differentiation, fibrosis and inflammation, as well as an oxidative stress-associated phenotype in rat ventricular CFs via *NFATc3 in a non-cytotoxic pathway*

Ventricular CFs were freshly isolated from adult male Wistar rats and maintained in primary culture for 3 days in the presence of 10% fetal bovine serum (FBS). Cells were then serum starved for 1 day before treating them for an additional 24 h with 10% FBS either alone or with cyclosporine A (CsA) and several concentrations of P.E. (extract of grape pomace polyphenol) whereas control cells remained without serum. Immunofluorescence on cultured CFs revealed a strong

expression of collagen 1 (COL1), the major ECM marker secreted by these cells (Supplementary Fig. S1A, D), with no presence of endothelial (CD31) or cardiomyocyte markers (MYH6) (Supplementary Fig. S1B–D), indicating consistently pure CFs cell preparations without contamination from other cardiac cell types.

Rat ventricular CFs treated with FBS presented a higher activation level of NFATc3, as reflected by the decrease in its phosphorylation when compared with control cells without serum (Fig. 1A). FBS also stimulated cell proliferation, as assessed by 3-(4,5-dimethylthiazol-2-yl)-2,5-diphenyltetrazolium bromide (MTT) (Fig. 1B), cell count (Fig. 1C), and cell cycle markers, that is, proliferating cell nuclear antigen (PCNA), KI67, and cyclin D1 (CCND1) (Fig. 1D) as well as migration (Fig. 1E). Oxidative stress, reflected by total intracellular reactive oxygen species (ROS), was also increased, as seen by 2′,7′-dichlorofluorescein (DCF) fluorescence signal (Fig. 1F) and a significant amount of nuclear RNA/DNA damage reflected by high 8-hydroxy-2′-deoxyguanosine (8-OHDG) staining colocalized with 4′,6-diamidino-2-phenylindole (DAPI) in the nuclei (Fig. 1G). 8-OHDG was also present in isolated mitochondria from CFs treated with FBS (Fig. 1H). CF secretory profile was affected by an increase in ECM major component, COL1, pro-fibrotic transforming growth factor beta 1 (TGF-β1), and pro-inflammatory interleukin 1 (IL1) (Fig. 1I). CF differentiation into myofibroblasts was also stimulated by FBS, as assessed by markers, that is, alpha smooth muscle actin (*α-SMA*), *COL1*, fibronectin 1 *(FN1)*, vimentin *(VIM)*, and embryonic smooth muscle myosin heavy chain *(SMEMB)* (Fig. 1J).

Several physiologically relevant low concentrations of P.E. were then tested on CFs and led to abrogation of NFATc3 activity (Fig. 1A), proliferation, and migration (Fig. 1B–E); total cellular as well as mitochondrial oxidative stress (Fig. 1F–H); and fibrotic, inflammatory, and differentiation markers (Fig. 1I, J) with concentration-dependent effects. Furthermore, to confirm NFATc3 necessity for CF proliferation, migration, differentiation, oxidative stress, and fibrotic phenotype, CsA was used and resulted in similar effects (Fig. 1A–J). Finally, activity of the Ca^{2+} and calmodulin-dependent serine/threonine phosphatase, calcineurin, which dephosphorylates and activates NFATc3, was evaluated in CFs. Cells treated with FBS released significant amounts of free phosphate, whereas P.E. and CsA treatments decreased calcineurin activity (Supplementary Fig. S2). These effects were mediated in a non-cytotoxic way, as revealed by trypan blue exclusion and propidium iodide tests (Supplementary Fig. S3A, B). Further confirmation was done by studying the expression of apoptotic genes, caspase 3 (*CASP3*; pro-), and B cell lymphoma 2 (*BCL2*; anti-) that remained stable under P.E. (Supplementary Fig. S3C, D). As a positive control, H_2O_2 treatment resulted in high cytotoxicity and apoptosis (Supplementary Fig. S3A, B).

P.E. decreases basal Ca^{2+} and receptor-operated Ca^{2+} entry but not store-operated Ca^{2+} entry in rat ventricular CFs

Basal Ca^{2+} level was studied in rat CFs. FBS increased Ca^{2+} levels as compared with control cells, whereas P.E. decreased them (Fig. 2A). The DAG-generating AngII and the DAG analog 1-oleoyl-2-acetyl-*sn*-glycerol (OAG) were used to stimulate receptor-operated Ca^{2+} entry (ROCE) *via* TRPC3 indirectly and directly, respectively. Large Ca^{2+} entries, in both amplitude and rate of rise, were observed on re-addition of extracellular

FIG. 1. TRPC3 blockade by P.E. inhibits fibrotic phenotype of rat ventricular CFs *via* NFATc3. CFs were cultured for 3 days in the presence of 10% FBS; then, they were serum starved for 1 day before treating them for an additional 1 day with 10% FBS either alone or with CsA and several concentrations of P.E., whereas control cells remained without serum. **(A)** Western blots and quantifications of pNFATc3 and NFATc3 in cultured rat ventricular CFs with *GAPDH* as an internal control ($n=3$). **(B)** CF proliferation estimated by MTT assay as a percentage of control; absorbance at 550 nm. **(C)** Representative light microphotographs of CFs and histograms representing cell numbers per square millimeter of culture well in each condition, before (baseline) and after treatments. Two cell fields were analyzed in each condition. **(D)** Gene expression of cell cycle regulators in cultured CFs with *GAPDH* as housekeeping gene. **(E)** Scratch wound-healing assay represented as number of migrating cells (CFs) per field. **(F)** Representative microphotographs of CFs showing DCF fluorescence at 515 nm and histograms representing quantification of the fluorescence signal in a.u. Two cell fields were analyzed in each condition. **(G)** Representative microphotographs of CFs stained with 8-OHDG (594 nm) and DAPI and histograms representing quantification of the fluorescence signal as cells per field. Two cell fields were analyzed in each condition. **(H)** Western blots and quantifications of mitochondrial 8-OHDG in cultured rat ventricular CFs with COX4 as an internal control; lack of GAPDH band indicates the absence of cytosolic protein contamination ($n=3$). **(I)** Fibrotic and inflammatory cytokine secretions by CFs assayed by sircol and ELISA and expressed in $\mu g/10^6$ cells for collagen and $ng/10^6$ cells for TGF-β1 and IL1. **(J)** Gene expression of myofibroblast and ECM markers *(α-SMA*, *COL1*, *FN1*, *VIM*, and *SMEMB)* with *GAPDH* as housekeeping gene. Magnifications in **(C, F, G)** $\times 100$. Scale bars in **(C, F, G)** 50 μm. All quantitative data are reported as mean ± SEM. Normal distribution of the values is checked by Shapiro-Wilk test. Kruskal-Wallis one-way ANOVA on ranks tests are performed for multiple comparisons of values followed by Mann-Whitney U tests. All values with $p<0.05$ are considered significant. $^*p<0.01$ *versus* Control; $^{\#}p<0.05$ *versus* FBS. Unedited gels for **(A, H)** are presented in Supplementary Figure S8. *α-SMA*, alpha smooth muscle actin; 8-OHDG, 8-hydroxy-2′-deoxyguanosine; ANOVA, analysis of variance; a.u., arbitrary units; CFs, cardiac fibroblasts; *COL1*, collagen 1; COX4, cytochrome c oxidase subunit 4; CsA, cyclosporine A; DAPI, 4′,6-diamidino-2-phenylindole; DCF, 2′,7′-dichlorofluorescein; ECM, extracellular matrix; ELISA, enzyme-linked immunosorbent assay; FBS, fetal bovine serum; *FN1*, fibronectin 1; GAPDH, glyceraldehyde-3-phosphate dehydrogenase; IL1, interleukin 1; MTT, 3-(4,5-dimethylthiazol-2-yl)-2,5-diphenyltetrazolium bromide; MW, molecular weight marker; NFATc3, nuclear factor of activated T cells c3; P.E., extract of grape pomace polyphenols; pNFATc3, phospho-NFATc3; SEM, standard error of the mean; *SMEMB*, embryonic smooth muscle myosin heavy chain; TGF-β1, transforming growth factor beta 1; TRPC3, transient receptor potential canonical 3; *VIM*, vimentin. Color images are available online.

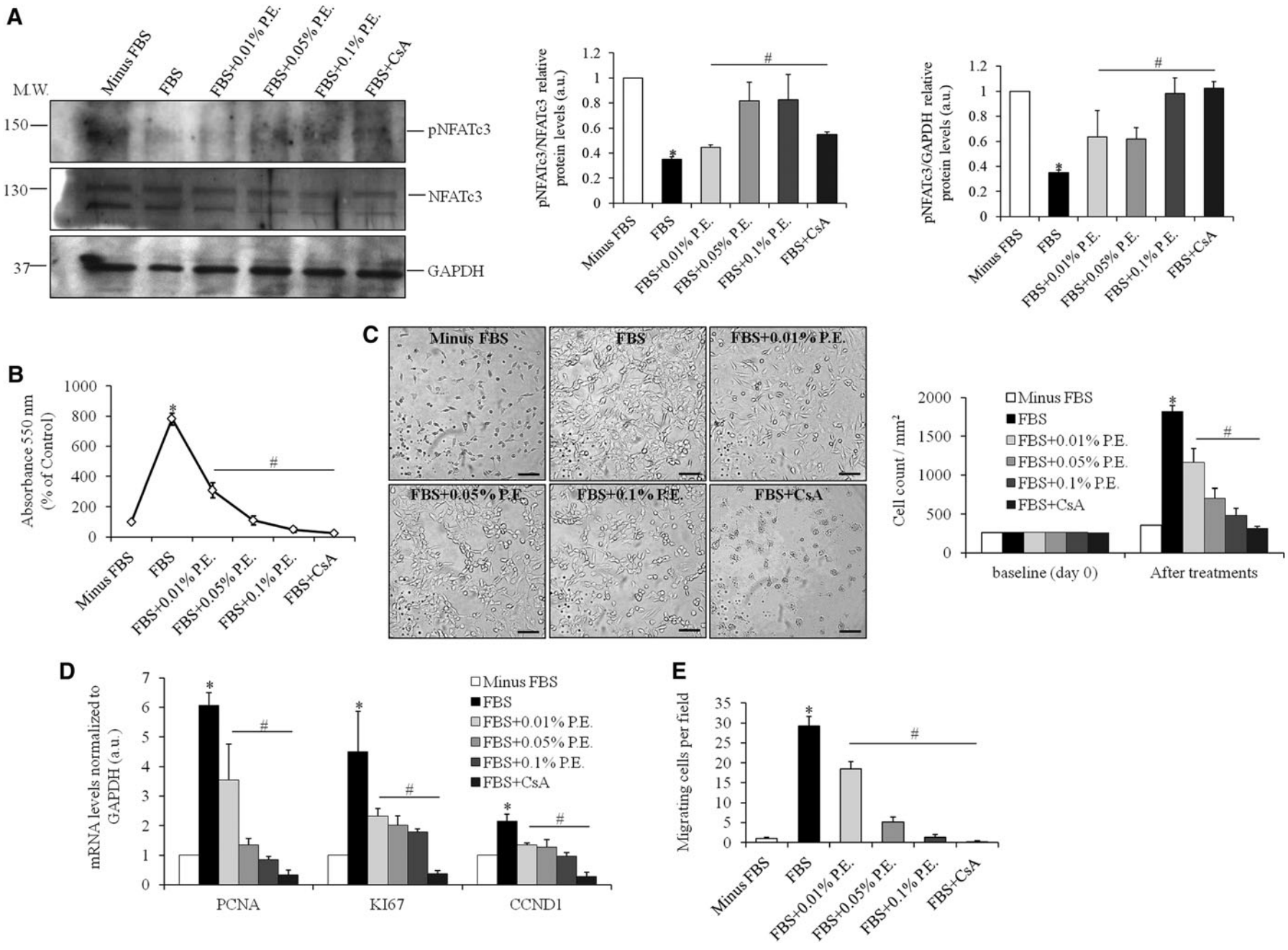
A
M.W.
Minus FBS
FBS
FBS+0.01% P.E.
FBS+0.05% P.E.
FBS+0.1% P.E.
FBS+CsA
150
130
37
pNFATc3
NFATc3
GAPDH
pNFATc3/NFATc3 relative protein levels (a.u.)
pNFATc3/GAPDH relative protein levels (a.u.)
B
Absorbance 550 nm (% of Control)
C
Minus FBS
FBS
FBS+0.01% P.E.
FBS+0.05% P.E.
FBS+0.1% P.E.
FBS+CsA
Cell count / mm²
baseline (day 0)
After treatments
D
mRNA levels normalized to GAPDH (a.u.)
PCNA
KI67
CCND1
E
Migrating cells per field

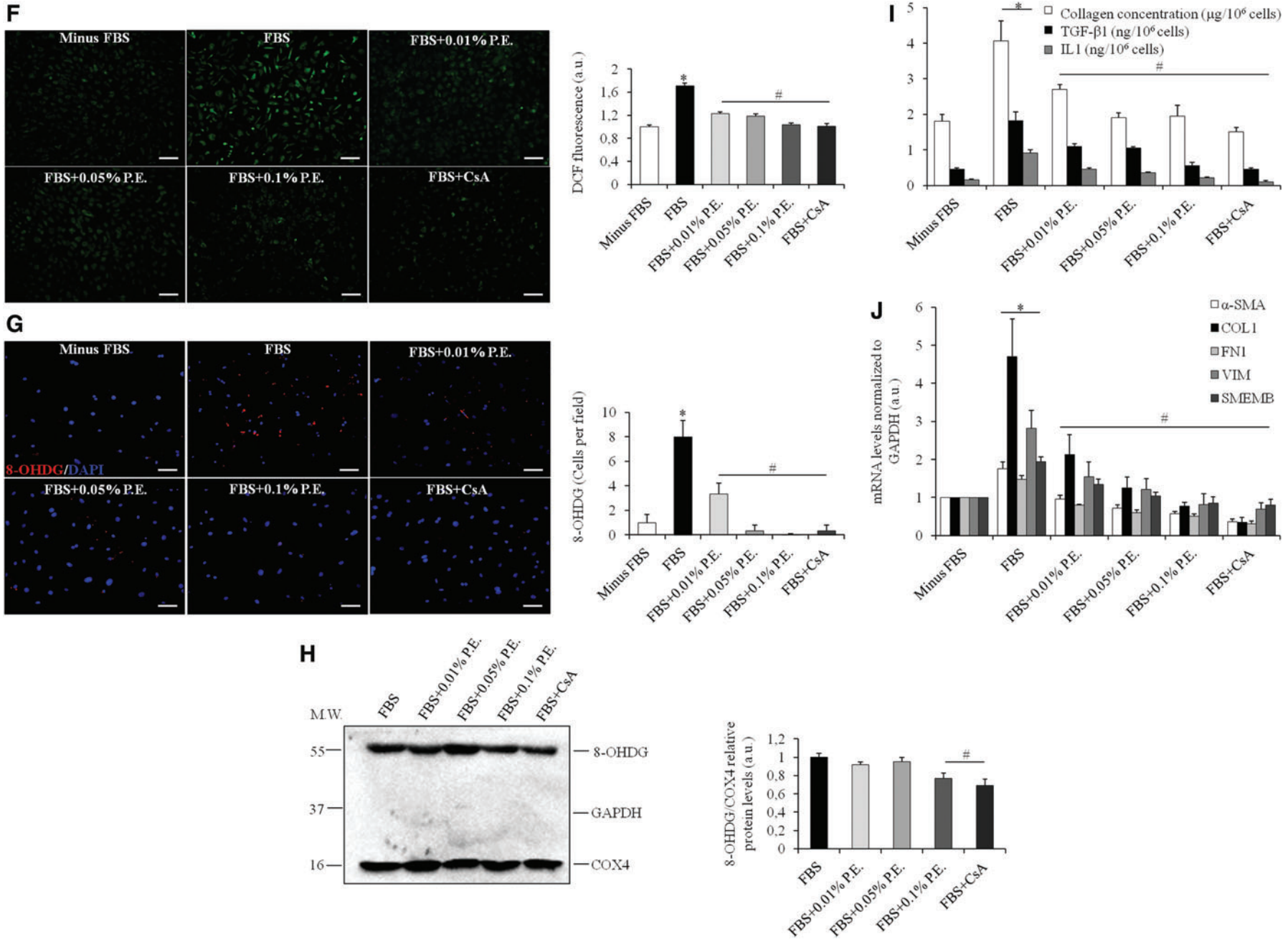

FIG. 1. *(Continued)*

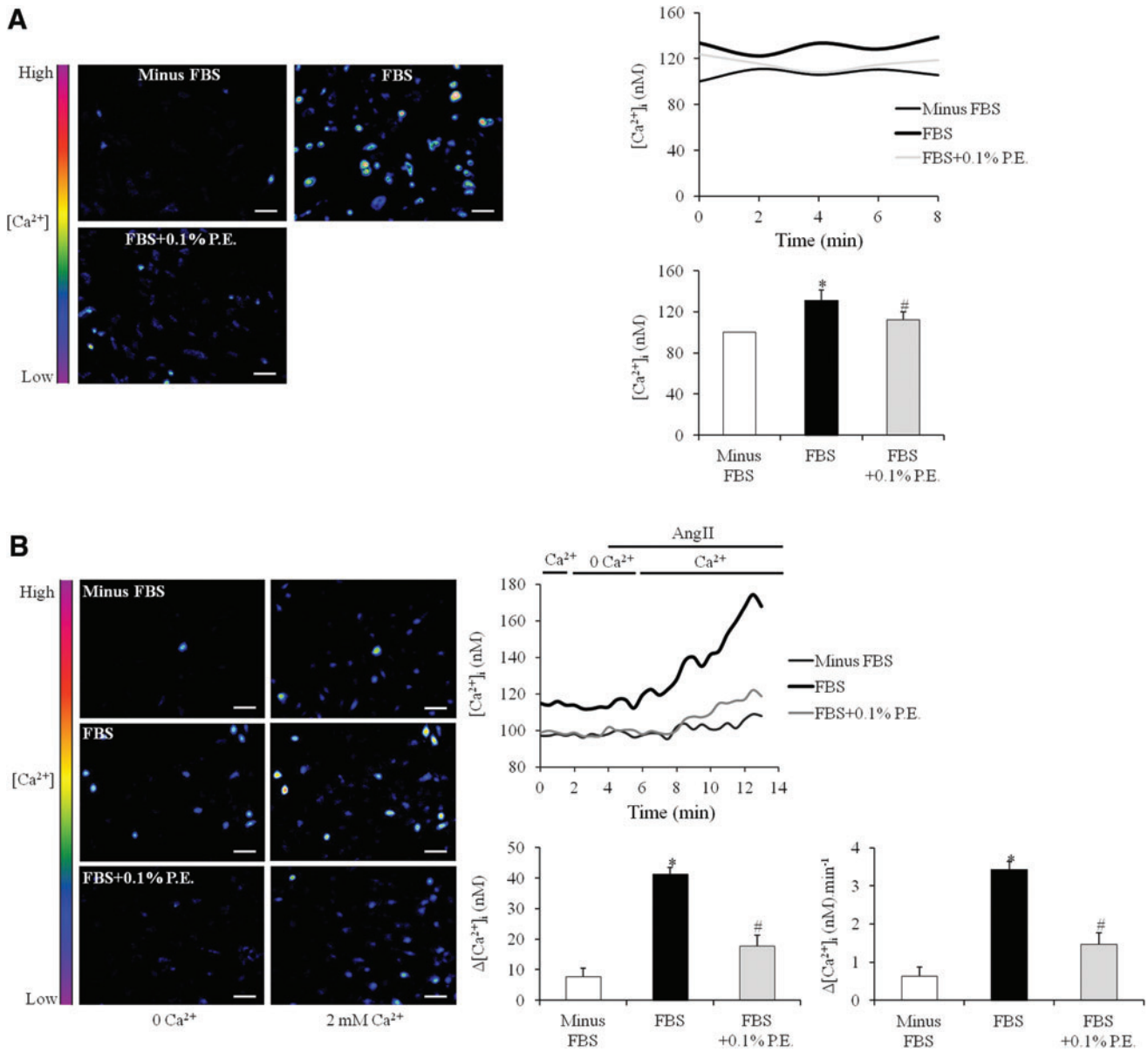

FIG. 2. Inhibition of basal Ca^{2+} and AngII-mediated ROCE in rat ventricular CFs by P.E. CFs were cultured for 3 days in the presence of 10% FBS; then, they were serum starved for 1 day before treating them for an additional 1 day with 10% FBS either alone or with 0.1% P.E., whereas control cells remained without serum. **(A)** Basal Ca^{2+} fluorescence microphotographs, traces, and quantifications in rat CFs. **(B, C)** AngII and OAG-mediated Ca^{2+} entries (ROCE) fluorescence microphotographs, traces, and quantifications reported as amplitudes ($\Delta[Ca^{2+}]_i$ [n*M*]) and rates of Ca^{2+} entry ($\Delta[Ca^{2+}]_i$ [n*M*]$\cdot min^{-1}$) in CFs. **(D)** Fluorescence microphotographs and traces of SOCE mediated by CPA and reported as amplitudes ($\Delta[Ca^{2+}]_i$ [n*M*]) and rates of Ca^{2+} entry ($\Delta[Ca^{2+}]_i$ [n*M*]$\cdot min^{-1}$) in CFs. All Ca^{2+} imaging data are an average from several cells ($n = 15$ cells) from one coverslip and are representative of several independent recordings ($n = 3$). Magnifications: $\times 100$. Scale bars: 50 μm. All quantitative data are reported as mean $\pm$ SEM. Normal distribution of the values is checked by Shapiro-Wilk test. Kruskal-Wallis one-way ANOVA on ranks tests are performed for multiple comparisons of values followed by Mann-Whitney U tests. All values with $p < 0.05$ are considered significant. $^{*}p < 0.05$ *versus* Control; $^{\#}p < 0.05$ *versus* FBS. AngII, angiotensin II; CPA, cyclopiazonic acid; OAG, 1-oleoyl-2-acetyl-*sn*-glycerol; ROCE, receptor-operated Ca^{2+} entry; SOCE, store-operated Ca^{2+} entry. Color images are available online.

Ca^{2+} in cells treated with FBS (Fig. 2B, C). CFs treated with P.E. presented abolished Ca^{2+} entries comparable to control cells (Fig. 2B, C). FBS treatment increased Ca^{2+} release from stores on addition of cyclopiazonic acid (CPA) and increased store-operated Ca^{2+} entry (SOCE) amplitude and rate of rise; however, P.E. did not affect either Ca^{2+} stores or SOCE (Fig. 2D).

Positive feedback loop between TRPC3 and NFATc3 driving rat ventricular CF fibrotic phenotype

To explain the observed effects of P.E. on Ca^{2+} entries in rat CFs, expression of TRPC3 was analyzed after P.E. treatment. FBS increased the channel expression whereas

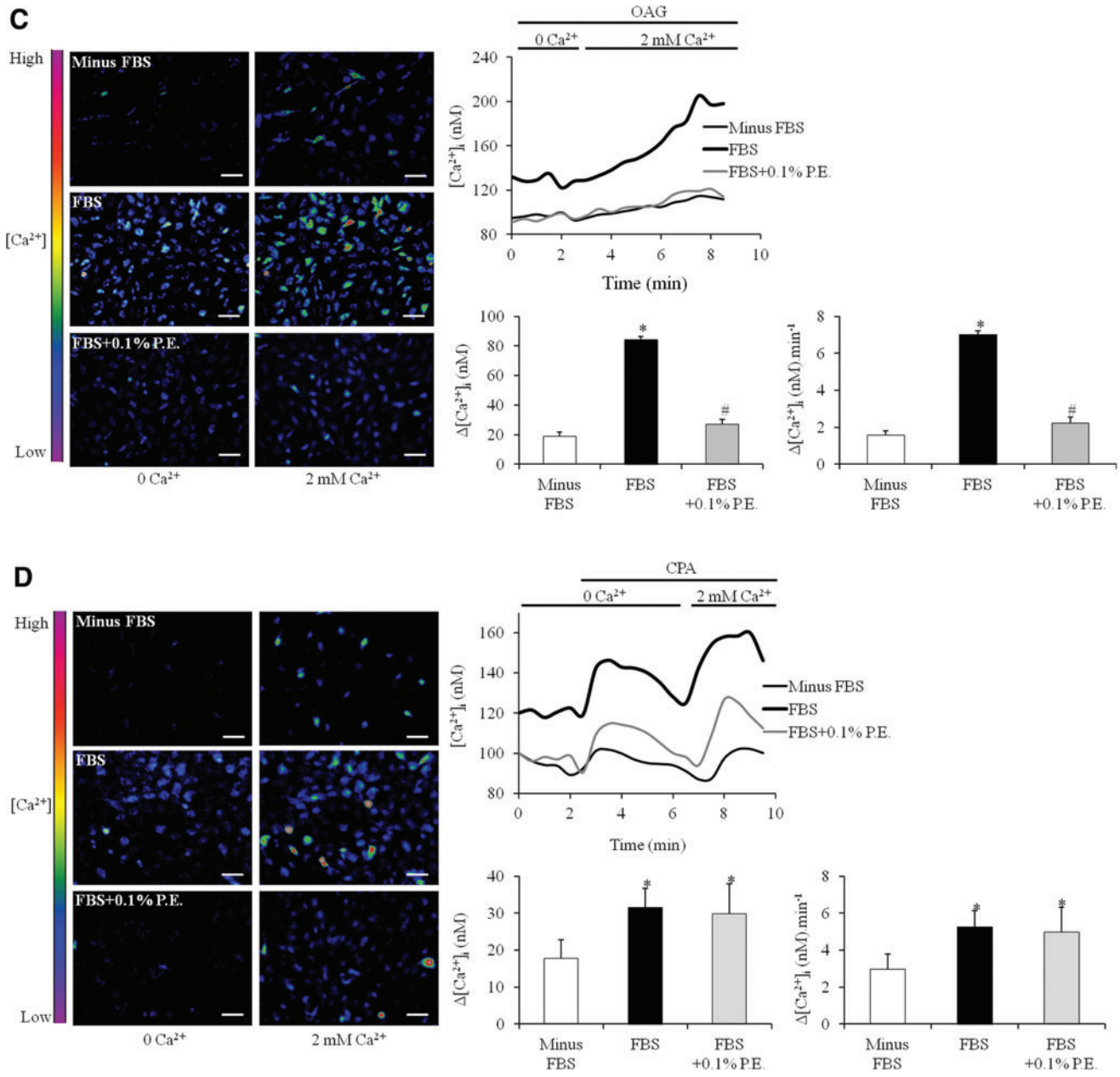

FIG. 2. *(Continued)*

P.E. decreased it in a concentration-dependent manner (Fig. 3A). To further validate the contribution of TRPC3 to the CF phenotype, specific pharmacological inhibition was performed by 10 μM N-[4-[3,5-Bis(trifluoromethyl)-1H-pyrazol-1-yl]phenyl]-4-methyl-benzenesulfonamide (Pyr10). Pyr10 decreased basal Ca^{2+} level and ROCE (Fig. 3B, C) while inhibiting CF proliferation (Fig. 3D). To eliminate a possible chelating interaction between gallic acid and intracellular Ca^{2+}, gallic acid with the same concentration as found in the grape pomace P.E. (18.8 nM) was acutely added on CFs without having any effect (Supplementary Fig. S4A). Different inhibitors of TRPC3 channels, that is, Pyr3, SKF96365, YM58483, and gadolinium (Gd^{3+}), were also tested and resulted in similar inhibitory effects on Ca^{2+}, with maximal effects seen with pan-TRPC inhibitors SKF96365, YM58483, and Gd^{3+} (Supplementary Fig. S4B–D). Finally, a positive feedback loop existed between TRPC3 and NFATc3 signaling, whereby blocking TRPC3 with Pyr10 inhibited NFATc3 activation (Fig. 3E) and blocking NFATc3 with several concentrations of CsA decreased the expression of TRPC3 (Fig. 3F).

P.E. effects on Ca^{2+} are mediated through a direct modulation of TRPC3 channels in rat ventricular CFs

To dissect the cause and consequence in TRPC3 and NFATc3 positive feedback loop modulation by P.E., we proceeded by acutely treating rat ventricular CFs with P.E. For this reason, cells cultured with FBS were stimulated with AngII and after Ca^{2+} levels increased, P.E. was added

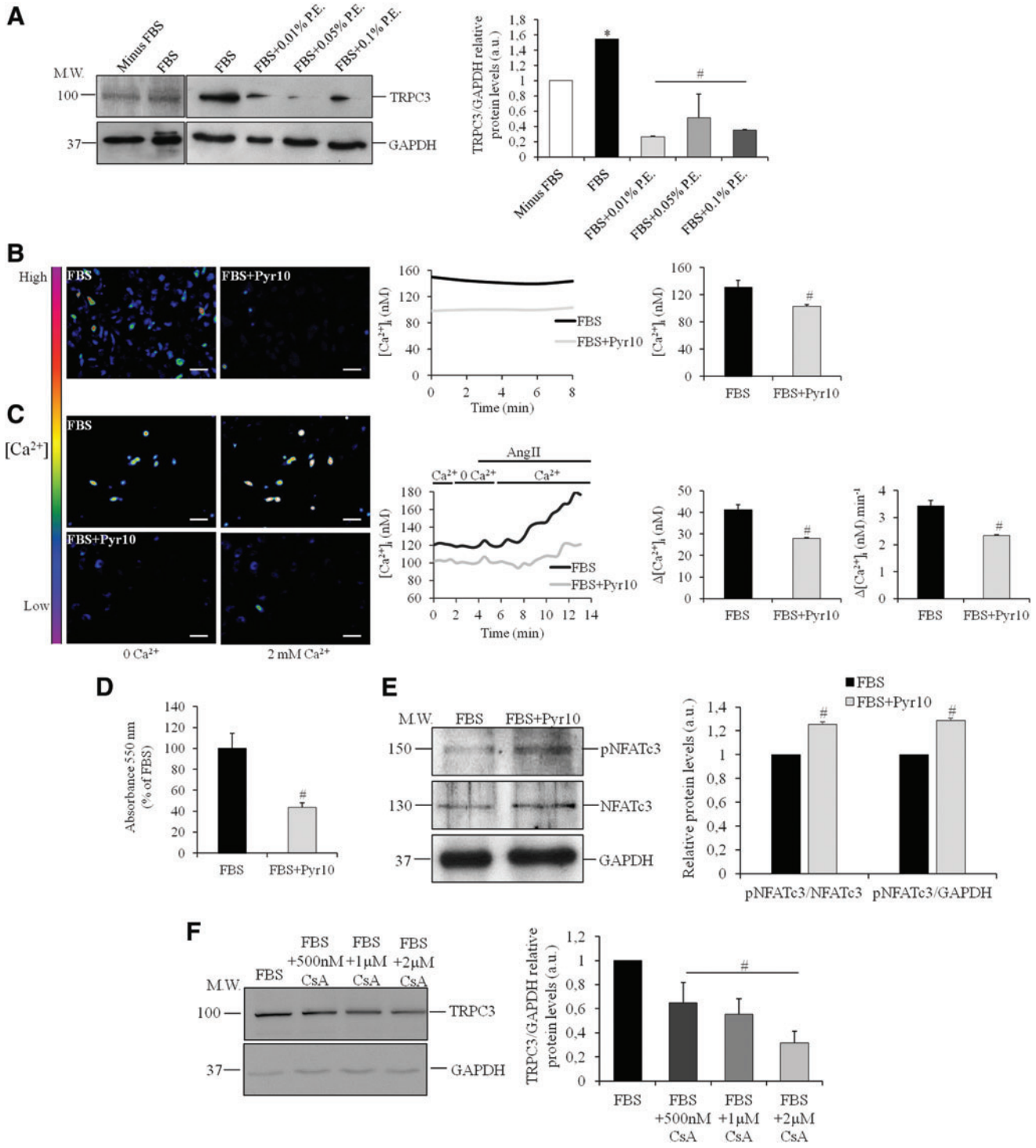

FIG. 3. TRPC3 mediates ROCE and fulfills a signaling circuit with NFATc3 in rat ventricular CFs. CFs were cultured for 3 days in the presence of 10% FBS; then, they were serum starved for 1 day before treating them for an additional 1 day with 10% FBS either alone or with Pyr10, several concentrations of P.E., and CsA whereas control cells remained without serum. **(A)** Western blots and quantifications of TRPC3 in cultured rat ventricular CFs with GAPDH as an internal control ($n = 3$). **(B, C)** Basal Ca^{2+} and AngII-mediated Ca^{2+} entries (ROCE) fluorescence microphotographs, traces, and quantifications reported as amplitudes ($\Delta[Ca^{2+}]_i$ [nM]) and rates of Ca^{2+} entry ($\Delta[Ca^{2+}]_i$ [n$M[\cdot \mathrm{min}^{-1}$) in CFs. **(D)** CF proliferation estimated by MTT assay as a percentage of control; absorbance at 550 nm. **(E, F)** Western blots and quantifications of pNFATc3, NFATc3, and TRPC3 in cultured rat ventricular CFs with GAPDH as an internal control ($n = 3$). All Ca^{2+} imaging data are an average from several cells ($n = 15$ cells) from one coverslip and are representative of several independent recordings ($n = 3$). Magnifications: $\times 100$. Scale bars: 50 μm. All quantitative data are reported as mean ± SEM. Normal distribution of the values is checked by Shapiro-Wilk test. Kruskal-Wallis one-way ANOVA on ranks test is performed for multiple comparisons of values followed by Mann-Whitney U test in **(A)**. Mann-Whitney U tests are performed when two conditions are compared in **(B–F)**. All values with $p < 0.05$ are considered significant. $^{*}p < 0.05$ *versus* Control; $^{\#}p < 0.05$ *versus* FBS. Unedited gels for **(A, E F)** are presented in Supplementary Figure S8. Pyr10, N-[4-[3,5-Bis(trifluoromethyl)-1H-pyrazol-1-yl]phenyl]-4-methyl-benzenesulfonamide. Color images are available online.

and led to a significant decrease in Ca^{2+} entry (Fig. 4A). To check whether this inhibitory effect of P.E was mediated by TRPC3, Pyr10 was added simultaneously with P.E. and did not lead to a further Ca^{2+} entry inhibition (Fig. 4A). Thereafter, CFs were pre-incubated for 5 min with P.E. before extracellular Ca^{2+} addition, which completely abrogated the increase in fluorescence signal (Fig. 4B). Combining Pyr10 with P.E. led to similar results (Fig. 4B). NFATc3 activation level was not affected in CFs treated for 5 min with P.E. (Fig. 4C).

P.E. ameliorates echocardiographic parameters, cardiac stress markers, and MF in L-NAME hypertensive rats in a blood pressure-independent manner

Systolic blood pressure began to significantly increase after 3 weeks of L-NAME treatment and continued to increase less steeply till the end of the protocol at 8 weeks as compared with sham-treated animals (Fig. 5A). P.E. treatment did not lower systolic blood pressure in L-NAME rats nor did it affect systolic blood pressure in sham animals (Fig. 5A). Blood pressure results were associated to a decrease in total expression of endothelial nitric oxide synthase (eNOS) as well as its phosphorylation level under L-NAME with a slight but non-significant increase under P.E. (Fig. 5B, C). However, P.E. increased eNOS expression and phosphorylation in sham rats (Fig. 5B, C).

Using the body surface area normalization method, according to the formula on Estimating of the Maximum Safe Starting Dose in Initial Clinical Trials for Therapeutics in Adult Healthy Volunteers issued by the US Food and Drug Administration, the $2\,mg\cdot kg^{-1}$ dose of P.E. used in this study corresponds to: Human equivalent dose (HED; $mg\cdot kg^{-1}$) = Animal equivalent dose ($mg\cdot kg^{-1}$) × (Animal km/Human km) = 2 × (6/37) = $0.324\,mg\cdot kg^{-1}$. This corresponds to a total of 22.68 mg P.E. for an adult of 70 kg.

Echocardiographic measurements revealed an increase in end-diastolic interventricular septal wall thickness (IVSTd) and end-diastolic left ventricular posterior wall thicknesses (LVPWd), with a decrease in left ventricular end-diastolic internal dimension (LVIDd) under L-NAME (Fig. 5D). Ejection fraction (EF) and heart weight/body weight ratio remained stable under L-NAME with a significant decrease in fractional shortening (FS) (Fig. 5E, F). P.E. normalized echocardiographic parameters and increased FS (Fig. 5D–F). Plasma cardiac (Troponin T, TnT, and brain natriuretic peptide, BNP), fibrotic (TGF-β1), and inflammatory tumor necrosis factor alpha, TNF-α, and C-reactive protein, CRP stress markers were all increased under L-NAME and lowered under P.E. (Fig. 5G–I). Histological analysis of cardiac sections revealed significant amounts of infiltrating leukocytes in hearts treated with L-NAME as compared with sham hearts (Fig. 5J). This was accompanied by an increase in MF and interstitial CF differentiation into myofibroblasts, as revealed by α-SMA labeling (Fig. 5J).

Further histological analysis of the location and extent of MF was then conducted on rat serial adjacent cardiac sections. Perivascular, sub-epicardial, and interstitial regions of the left ventricle myocardium were examined for total collagen deposition; perivascular fibrosis was defined as collagen accumulation in the adventitia of coronary arteries. Sham rats had coronary vessels with thin adventitia, and no signs of sub-epicardial or interstitial fibrosis. Very few cells that stained positive for PDGFRα and TCF21 were present in the three studied regions (Supplementary Fig. S5A, B, E). After treatment with L-NAME, rats developed perivascular, sub-epicardial, and interstitial fibrosis, with sparse myocardial necrotic regions. Fibrotic regions presented dense and increased cellular labeling for PDGFRα and TCF21, and both markers seemed to localize in the same subset of CF populations, indicating increased epicardial progenitor marker expression and distribution (Supplementary Fig. S5C, E). These histological changes were all ameliorated under P.E. and hearts were comparable to sham, with regression in the number and extent of PDGFRα and TCF21-positive cells (Fig. 5J and Supplementary Fig. S5D, E). When CF Trpc3 messenger RNA (mRNA) expression was plotted against interstitial fibrosis and FS, significant correlations were found (Fig. 5K, L).

P.E. treatment reduces in vivo *ventricular CF activation by modulating the TRPC3-NFATc3 pathway in L-NAME hypertensive rats*

CFs isolated from L-NAME-treated hearts showed marked increases in proliferation (Fig. 6A), fibrotic activity (Fig. 6B, C), differentiation into myofibroblasts as assessed by the high expression of *COL1*, α-*SMA*, and *FN1* (Fig. 6D), as well as oxidative stress with increased DCF and 8-OHDG fluorescence labeling (Fig. 6E, F) in comparison to sham hearts. This was associated to increased NFATc3 activation (Fig. 6G) and higher TRPC3 expression (Fig. 6H). High basal Ca^{2+} (Fig. 6I) and ROCE AngII-mediated TRPC3 Ca^{2+} influx were also recorded in CFs isolated from L-NAME hearts (Fig. 6J, K). When cells were treated with Pyr10, large decreases in basal Ca^{2+} and ROCE were observed in comparison to cells from the other groups (Fig. 6I–K), further demonstrating the importance of TPPC3 inhibition in the observed effects of P.E. Proliferative and fibrotic activities of L-NAME CFs were drastically reduced under P.E. treatment (Fig. 6A–C), and decreases were also noted in differentiation markers and oxidative stress (Fig. 6D–F). The TRPC3-NFATc3 pathway was also normalized in L-NAME CFs under P.E. as shown by the respective decrease in protein expression and dephosphorylation (Fig. 6G, H) as well as TRPC3 channel activity (Fig. 6I–K).

Pharmacological inhibition and genetic deletion of TRPC3 in mice protect against MF induced by L-NAME in a blood pressure-independent manner

To further validate the role of TRPC3 in driving CF activation and leading to MF, the same L-NAME model was used in mice treated with Pyr10 and $TRPC3^{-/-}$ mice. Similarly, L-NAME increased systolic blood pressure after 3 weeks of treatment; however, neither Pyr10 treatment nor TRPC3 knockout affected blood pressure (Fig. 7A). eNOS phosphorylation levels in abdominal aorta decreased in all L-NAME-treated groups, with no effect of TRPC3 blockade (Fig. 7B). Changes in left ventricular parameters were noted under L-NAME, despite a preserved heart weight/body weight ratio and EF (Fig. 7C–E); septal and posterior wall thicknesses increased, whereas chamber diameter and FS decreased (Fig. 7C–E). Histological analysis revealed significant amounts of infiltrating leukocytes in hearts treated with L-NAME as compared with sham hearts (Fig. 7F) with an increase in total myocardial collagen (Fig. 7G).

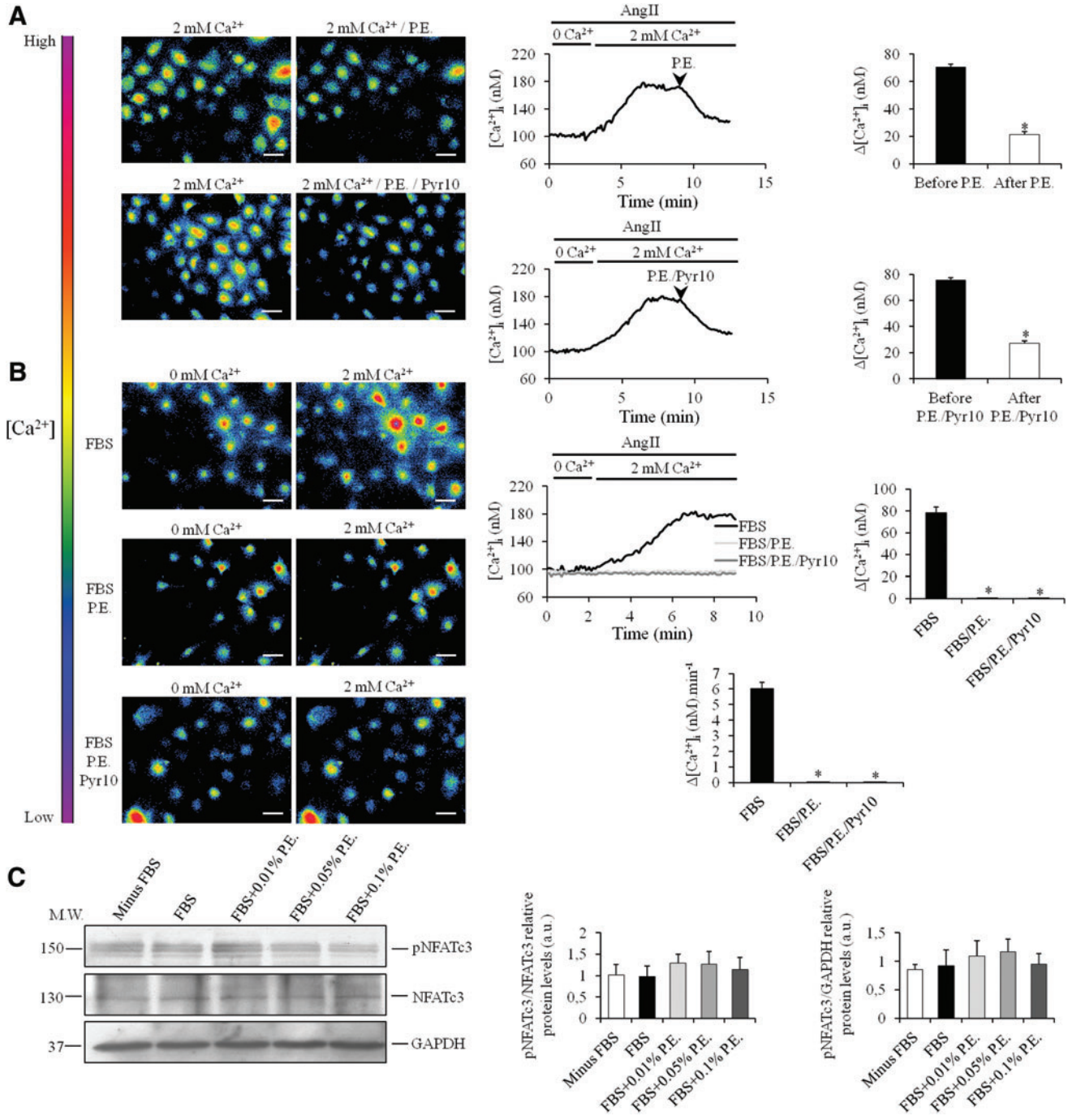

FIG. 4. P.E. acutely modulates TRPC3 channel activity but not NFATc3 phosphorylation in rat ventricular CFs. CFs were cultured for 3 days in the presence of 10% FBS; then, they were serum starved for 1 day before treating them for an additional 1 day with 10% FBS. P.E. and Pyr10 were either added acutely after Ca^{2+} entry or pre-incubated for 5 min with cells before extracellular Ca^{2+} re-addition. **(A)** AngII-mediated Ca^{2+} entry (ROCE) fluorescence microphotographs, traces, and quantifications reported as amplitudes ($\Delta[Ca^{2+}]_i$ [n*M*]) in CFs. *Black arrows* indicate the time of P.E. and P.E./Pyr10 acute addition during the perfusion protocol. **(B)** AngII-mediated Ca^{2+} entry (ROCE) fluorescence microphotographs, traces, and quantifications reported as amplitudes ($\Delta[Ca^{2+}]_i$ [n*M*]) in CFs pre-incubated for 5 min with either P.E. or P.E./Pyr10 before extracellular Ca^{2+} re-addition. **(C)** Western blots and quantifications of pNFATc3 and NFATc3 in cultured rat ventricular CFs treated for 5 min with P.E., with GAPDH as an internal control ($n = 3$). All Ca^{2+} imaging data are an average from several cells ($n = 15$ cells) from one coverslip and are representative of several independent recordings ($n = 3$). Magnifications in **(A, B)** $\times 100$. Scale bars in **(A, B)** 50 μm. All quantitative data are reported as mean $\pm$ SEM. Normal distribution of the values is checked by Shapiro-Wilk test. Kruskal-Wallis one-way ANOVA on ranks tests are performed for multiple comparisons of values followed by Mann-Whitney U tests. All values with $p < 0.05$ are considered significant. $^*p < 0.05$ *versus* before P.E., before P.E./Pyr10, and FBS, respectively. Unedited gels for **(C)** are presented in Supplementary Figure S8. Color images are available online.

L-NAME induced a similar pattern of MF in mice as seen in rats, with increases in perivascular, sub-epicardial, interstitial, and necrotic region replacement collagen deposition as compared with sham wild-type (WT) mice (Supplementary Fig. S6A, B, F). To determine whether developmental mechanisms are reactivated in these fibrotic regions with induction of embryonic epicardial progenitor markers, expression of PDGFRα and TCF21 was examined. As compared with sham mice, where few cells labeled positive for these markers, L-NAME-treated mice showed an increase in the number and distribution of PDGFRα and TCF21 in all fibrotic regions, especially in the necrotic myocardium where cardiomyocytes were completely replaced by CFs expressing these markers (Supplementary Fig. S6A, B, F).

When L-NAME was administered to WT mice treated with Pyr10 or TRPC3$^{-/-}$ mice, a complete abrogation of MF was observed, with thin coronary vessels thickness and absence of necrotic regions with replacement collagen. Epicardial progenitor markers were present in a similar pattern as with sham WT and sham TRPC3$^{-/-}$ mice (Supplementary Fig. S6C–F).

Ventricular CFs from Pyr10-treated and TRPC3$^{-/-}$ hypertensive mice exhibit decreased activation

CFs isolated from L-NAME hearts exhibited an increase in NFATc3 activation (Fig. 8A) and possessed a higher proliferative phenotype than cells isolated from sham hearts (Fig. 8B). These cells had a higher basal Ca^{2+} level (Fig. 8C) with an increase in ROCE (Fig. 8D). L-NAME WT mice treated with Pyr10 and TRPC3$^{-/-}$ mice presented lower levels of NFATc3 activation (Fig. 8A), proliferation rate (Fig. 8B), basal Ca^{2+} (Fig. 8C), and ROCE (Fig. 8D).

TRPC3 is functional in human ventricular CFs and upregulated in MF

Myocardium samples were obtained from patients, aged 38–80 years with an average of 63.8 years, who underwent valve replacement surgeries. Patients with non-failing hearts ($n=7$) had EFs ranging from 60% to 65% with an average of $62.57\% \pm 0.95\%$. Patients with failing hearts ($n=6$) had either a slightly decreased EF (heart failure with preserved EF) or a severely depressed function (heart failure with reduced EF), with values ranging from 30% to 50% and an average of $42.6\% \pm 3.1\%$ (Supplementary Table S1). Ventricular CFs isolated from failing hearts presented higher expression of ECM and myofibroblast markers, *COL1*, collagen 3 *(COL3)*, *FN1*, and *α-SMA* as compared with cells from non-failing hearts (Fig. 9A).

Expression and distribution of epicardial progenitor transcription factors, PDGFRα and TCF21, were also studied. Many interstitial cells stained positive for the two proteins in non-failing as well as failing hearts with no significant differences in the respective patterns (Fig. 9B, C). However, prominent interstitial fibrosis was present in the failing group only (Fig. 9B). Collagen deposition and developmental reactivation markers were only studied in the interstitium since epicardial and perivascular biopsies were not possible. TRPC3 was localized within the myocardial interstitium with the absence of expression in cardiomyocytes (Fig. 9D). TRPC3 interstitial expression increased in fibrotic areas and double immunofluorescence showed a colocalization with COL1, further confirming the interstitial presence of this channel (Fig. 9E). CFs from failing hearts presented a higher expression of TRPC3 and COL1 as compared with non-failing hearts, and the channel expression correlated with the increase in the ECM marker (Fig. 9F). Ca^{2+} entries were elicited by AngII on the addition of extracellular Ca^{2+} and Ca^{2+} level correlated with TRPC3 expression level in human CFs (Fig. 9G).

Pharmacological modulation of TRPC3-NFATc3 decreases proliferation and collagen secretion of human ventricular CFs in vitro

FBS increased TRPC3 expression and NFATc3 dephosphorylation (Fig. 10A) with similar effects on proliferation (Fig. 10B) and collagen secretion (Fig. 10C) as compared with

FIG. 5. P.E. attenuates MF in L-NAME hypertensive rats independently of blood pressure regulation. Rats were treated for 8 weeks with L-NAME and P.E.; then, hearts, abdominal aorta, and plasma were collected for further analysis. **(A)** Systolic blood pressure (mmHg) measured non-invasively by tail-cuff in the different groups of rats during the 8-week treatments. **(B, C)** Western blots and quantifications of eNOS and p-eNOS, respectively, in abdominal aorta, with GAPDH as an internal control ($n=3$). **(D–F)** Echocardiographic left ventricular parameters (IVSTd, LVIDd, and LVPWd in cm; EF and FS in %) and heart weight/body weight ratio (mg/g) in the different groups of rats after the 8-week treatments. **(G–I)** Plasma cardiac (TnT and BNP), fibrotic (TGF-β1), and inflammatory (TNF-α and CRP) stress markers measured by ELISA. **(J)** Representative microphotographs of rat left ventricular sections stained with either hematoxylin/eosin or Masson's trichrome and labeled with α-SMA by immunohistochemistry, as well as histograms showing semi-quantitative scores of infiltrating leukocytes per section field, fibrotic areas (%), and α-SMA expression in a.u. *Black arrows* show infiltrating leukocytes. Sections are of 4 μm thickness. Two sections were analyzed in each condition in animals. **(K, L)** Correlation between fibrotic area, FS, and *Trpc3* mRNA expression, respectively, in ventricular CFs. Magnifications in **(J)** $\times 100$. Scale bars in **(J)** 50 μm. All quantitative data are reported as mean ± SEM. Normal distribution of the values is checked by Shapiro-Wilk test. Kruskal-Wallis one-way ANOVA on ranks tests are performed for multiple comparisons of values followed by Mann-Whitney U tests. Two-way ANOVA tests are performed followed by *post hoc* Holm-Sidak tests for blood pressure measurements. Pearson correlation coefficient is used to measure the strength of the relationship between fibrotic area, FS, and *Trpc3* mRNA expression. All values with $p<0.05$ are considered significant. $^{*}p<0.05$ *versus* Sham and Sham P.E.; $^{\#}p<0.05$ *versus* L-NAME. Unedited gels for **(B, C)** are presented in Supplementary Figure S9. BNP, brain natriuretic peptide; CRP, C-reactive protein; EF, ejection fraction; eNOS, endothelial nitric oxide synthase; FS, fractional shortening; HE, hematoxylin/eosin; IVSTd, end-diastolic interventricular septal wall thickness; L-NAME, N(ω)-nitro-L-arginine methyl ester; LVIDd, left ventricular end-diastolic internal dimension; LVPWd, end-diastolic left ventricular posterior wall thickness; MF, myocardial fibrosis; mRNA, messenger RNA; MT, Masson's trichrome; p-eNOS, phospho-eNOS; TNF-α, tumor necrosis factor alpha; TnT, troponin T. Color images are available online.

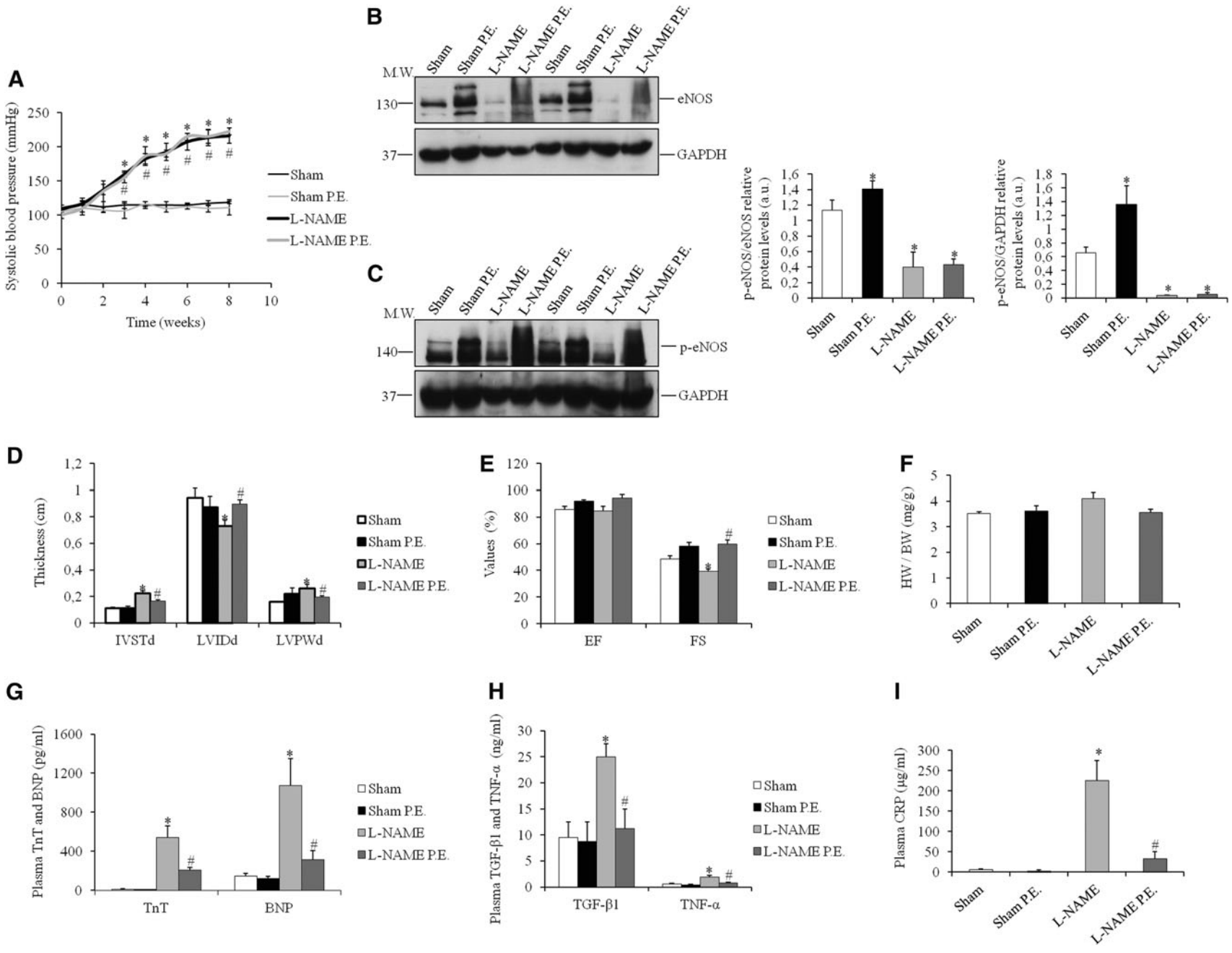
A
Systolic blood pressure (mmHg)
Time (weeks)
Sham
Sham P.E.
L-NAME
L-NAME P.E.
B
M.W.
Sham
Sham P.E.
L-NAME
L-NAME P.E.
130
eNOS
37
GAPDH
C
140
p-eNOS
p-eNOS/eNOS relative protein levels (a.u.)
p-eNOS/GAPDH relative protein levels (a.u.)
D
Thickness (cm)
IVSTd
LVIDd
LVPWd
E
Values (%)
EF
FS
F
HW / BW (mg/g)
G
Plasma TnT and BNP (pg/ml)
TnT
BNP
H
Plasma TGF-β1 and TNF-α (ng/ml)
TGF-β1
TNF-α
I
Plasma CRP (μg/ml)

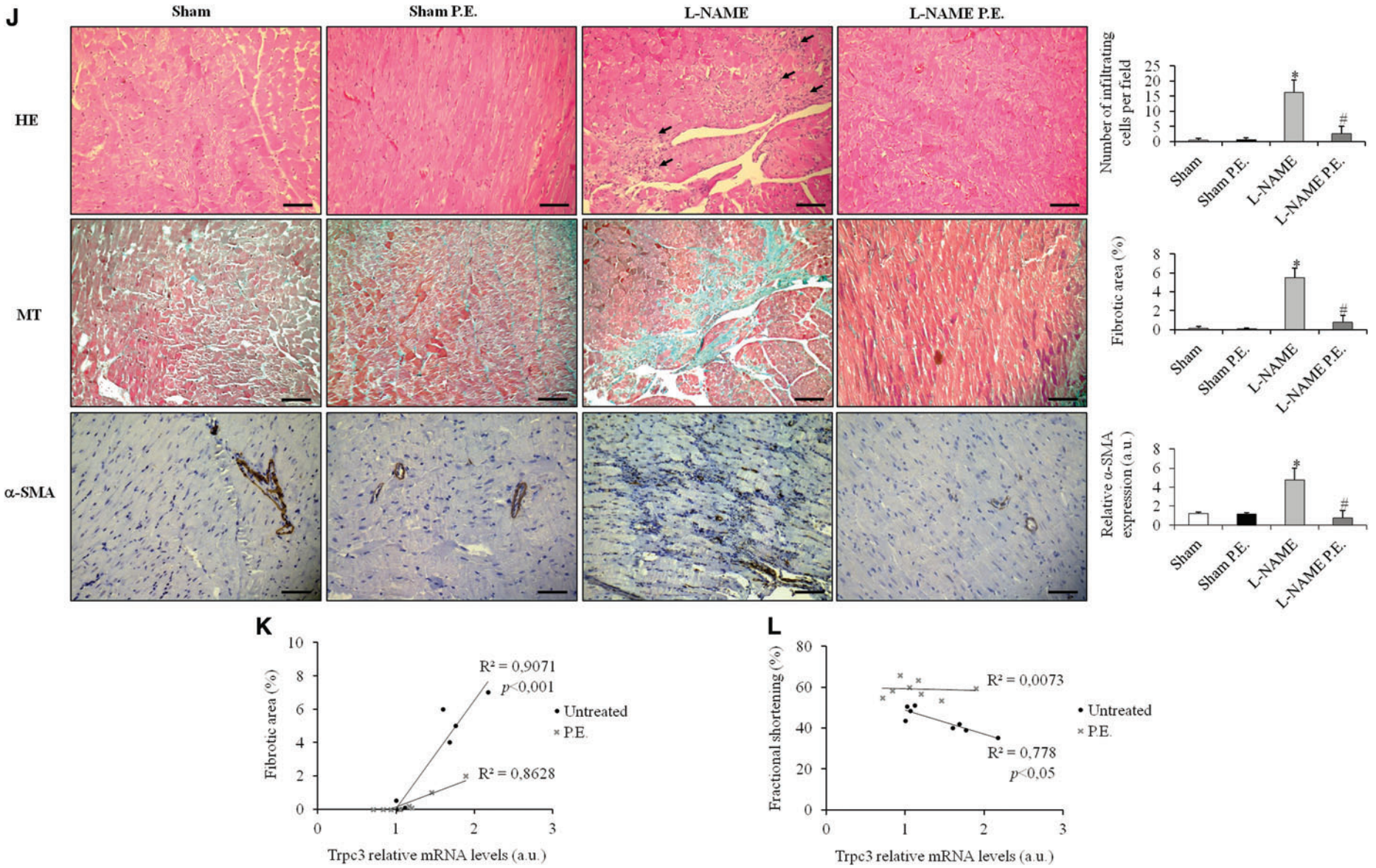

FIG. 5. *(Continued)*

control cells with serum-free medium. This was accompanied by an increase in basal Ca^{2+} level (Fig. 10D) and Ca^{2+} stimulated by AngII as compared with control cells (Fig. 10E). CFs were then treated with a low P.E. concentration that decreased TRPC3 expression, NFATc3 activation, proliferation, collagen secretion, as well as basal Ca^{2+} level and ROCE. Specific TRPC3 blockade by Pyr10 and NFATc3 inhibition by CsA displayed similar effects (Fig. 10A–E).

Discussion

Nearly all etiologies of heart disease summoned in MF are characterized by excessive deposition of ECM by ventricular CFs disrupting myocardial architecture, thus leading to overt heart failure (65). Limited knowledge of CF physiology continues to hinder progress in the development of meaningful new therapies targeting MF and inevitably leading to significant advancements in the treatment of heart failure. No studies have shown the role of TRPC3-NFATc3 of CF in human MF and whether its modulation either by targeted pharmacology and genetic ablation or by Ca^{2+}-modulatory cardiovascular health-promoting polyphenols would limit disease progression in animal models.

In this work, we checked whether modulation of this pathway would suppress the CF fibrotic phenotype *in vitro* and ameliorate MF *in vivo* in rodents, and we studied the functional relevance of this pathway in human ventricular CFs and its association to MF. The polyphenols mix used in this study seemed to be advantageous, owing to the possibility of synergistic interactions among multiple ingredients leading to enhanced bioactivity and bioavailability.

Increasing evidence is implicating CF and more precisely the activated CF, the myofibroblast, as a major pathological contributor in heart failure. Thus, dissecting CF biology and pathological signaling pathways remain an important component in the development of successful therapeutic strategies. TRPs channels have long emerged as central determinants of a vast array of physiological and pathophysiological processes at the cardiovascular level (68, 71). Animal studies showed the implication of these channels and the subsequent NFATc3 signaling pathway in ventricular CFs (6, 14, 37, 39). However, the presence of such channels in human ventricular CFs and their relevance to MF remain to be elucidated. Extensive interstitial fibrosis was present in failing hearts with high CF expression of ECM markers; however, expression and distribution of epicardial progenitor transcription factors, PDGFRα and TCF21, were comparable to non-failing hearts. TCF21 has been shown to be expressed in human cardiac fibrosis (1), but no data exist on the extent of expression in normal hearts. In rodents, the presence of PDGFRα and TCF21-positive cells in fibrotic areas depends on the injury stage of the heart, whereby expression increases on infarction, subsides in activated myofibroblasts, and finally returns to normal in late scars (20). Since it is difficult to evaluate the lifetime of the fibrotic tissue in human hearts, we hypothesize that myocardial biopsies from failing hearts in our study involved late-stage inactive sites of fibrosis. TRPC3 presented an interstitial expression and colocalized with collagen; moreover, the channel expression and function were increased in CFs from failing hearts.

CFs are very labile cells that spontaneously differentiate into myofibroblasts in long-term cultures (53), resulting in highly heterogeneous cultures (11). To circumvent this issue, we conducted all the *in vitro* experiments on freshly isolated CFs that were cultured for only 3 days and maintained their fibroblast characteristics. Human ventricular CFs expressed high levels of TRPC3, and channel expression was induced by FBS. Since AngII plays an important role in the progression of heart failure, possesses pro-fibrotic properties (34), and activates TRPCs channels (42), we assessed TRPC3 inhibition on AngII-mediated Ca^{2+} entry and consequent NFATc3 activation. TRPC3 modulation by P.E. and Pyr10 blocked the rise in Ca^{2+} elicited by AngII, inhibited NFATc3 activity as well as CF proliferation and collagen secretion.

TRPC3-NFATc3 pathway modulation by P.E. and Pyr10/CsA was further characterized in rat cultured ventricular CFs. First, P.E. treatment resulted in the abrogation of the CF fibrotic phenotype with significant decreases in proliferation, migration, oxidative stress, differentiation markers, and inflammatory and ECM component secretions. Ca^{2+} is critical for mitochondrial function, and TRPC3 has been shown to play a role in mitochondrial Ca^{2+} uptake (13, 18, 70), whereas mitochondrial Ca^{2+} overload is present in heart disease, generating ROS and worsening the disease (56). Thus, oxidative stress in the mitochondria of CFs was also evaluated by 8-OHDG expression that revealed a decrease in ROS with P.E. treatment. However, when compared with total cellular oxidative stress, mitochondrial 8-OHDG decreased only with high concentrations of P.E., suggesting that the mitochondrial compartment was less affected by P.E. as compared with cytosol and nucleus. NADPH oxidase (Nox) are important sources for ROS generation, and an intimate

FIG. 6. TRPC3-NFATc3 inhibition by P.E. suppresses *in vivo* ventricular CF activation in L-NAME hypertensive rats. Rats were treated for 8 weeks with L-NAME and P.E.; then, CFs were isolated for further analysis. **(A)** CF proliferation estimated by MTT assay as a percentage of sham; absorbance at 550 nm. **(B, C)** Fibrotic secretions by isolated CFs assayed by sircol and ELISA and expressed in $\mu g/10^6$ cells for collagen and $ng/10^6$ cells for TGF-β1. **(D)** Gene expression of myofibroblast and ECM markers (*COL1*, *α-SMA*, *FN1*) with *GAPDH* as housekeeping gene. **(E, F)** Histograms representing quantification of the fluorescence signals for DCF (at 515 nm; a.u.) and 8-OHDG (at 594 nm; cells per field) in isolated CFs. Two cell fields were analyzed in each condition. **(G, H)** Western blots and quantifications of pNFATc3, NFATc3, and TRPC3, in isolated CFs, with GAPDH as an internal control ($n=3$). **(I–K)** Basal Ca^{2+} and AngII-mediated Ca^{2+} entries (ROCE) quantifications reported as amplitudes ($\Delta[Ca^{2+}]_i$ [n*M*]) and rates of Ca^{2+} entry ($\Delta[Ca^{2+}]_i$ [n*M*]$\cdot min^{-1}$) in isolated CFs. All Ca^{2+} imaging data are an average from several cells ($n=15$ cells) from one coverslip and are representative of several independent recordings ($n=3$). All quantitative data are reported as mean ± SEM. Normal distribution of the values is checked by Shapiro-Wilk test. Kruskal-Wallis one-way ANOVA on ranks tests are performed for multiple comparisons of values followed by Mann-Whitney U tests. All values with $p<0.05$ are considered significant. $^{*}p<0.05$ *versus* Sham and Sham P.E.; $^{\#}p<0.05$ *versus* L-NAME; $\$p<0.05$ *versus* Sham, Sham P.E., L-NAME and L-NAME P.E. without Pyr10. Unedited gels for **(G, H)** are presented in Supplementary Figure S9.

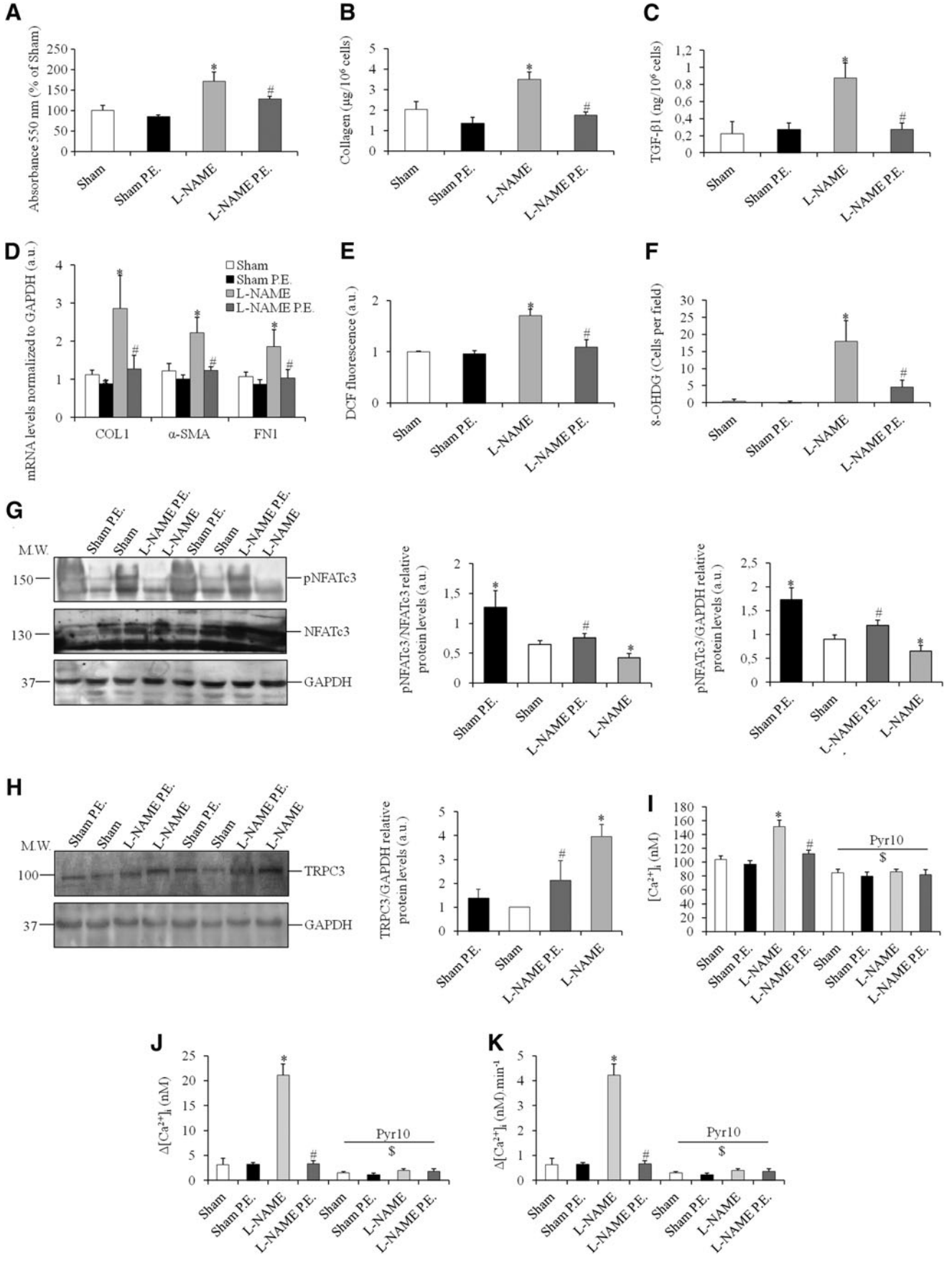
A
Absorbance 550 nm (% of Sham)
Sham
Sham P.E.
L-NAME
L-NAME P.E.
B
Collagen (µg/10⁶ cells)
C
TGF-β1 (ng/10⁶ cells)
D
mRNA levels normalized to GAPDH (a.u.)
COL1
α-SMA
FN1
E
DCF fluorescence (a.u.)
F
8-OHDG (Cells per field)
G
M.W.
pNFATc3
NFATc3
GAPDH
pNFATc3/NFATc3 relative protein levels (a.u.)
pNFATc3/GAPDH relative protein levels (a.u.)
H
TRPC3
TRPC3/GAPDH relative protein levels (a.u.)
I
[Ca²⁺]i (nM)
Pyr10
$
J
Δ[Ca²⁺]i (nM)
K
Δ[Ca²⁺]i (nM) min⁻¹

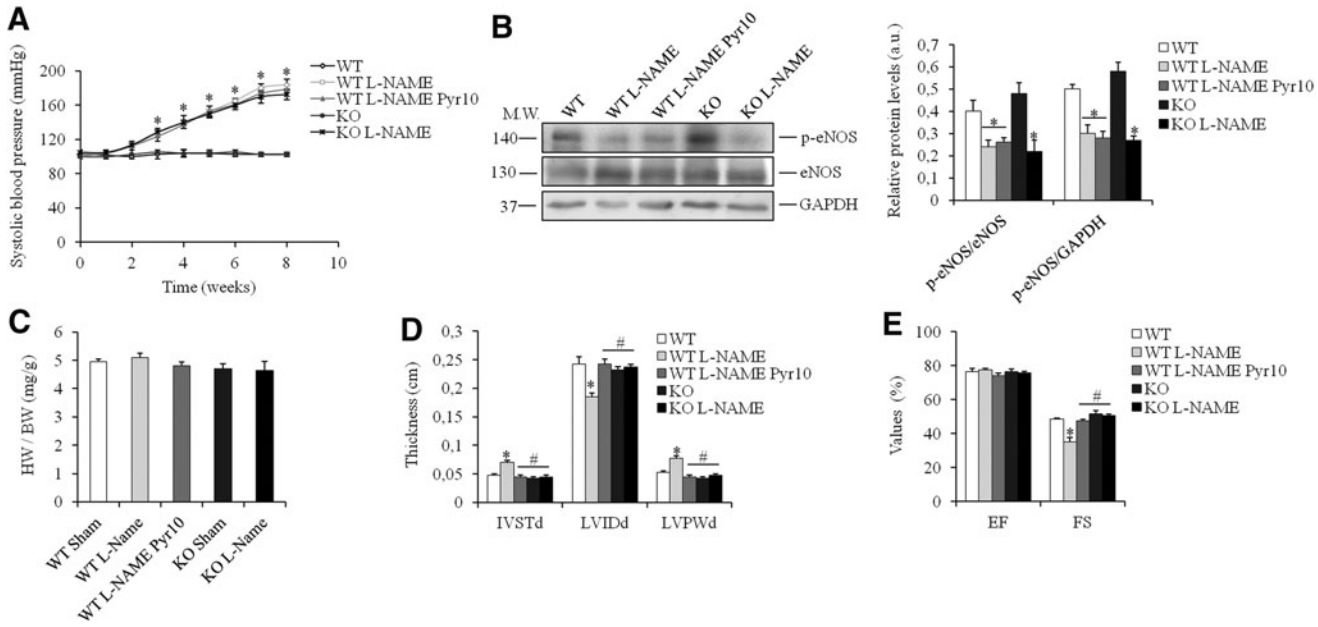

FIG. 7. Mice treated with Pyr10 and TRPC3$^{-/-}$ mice are protected against L-NAME-induced MF independently of blood pressure. Mice were treated for 8 weeks with L-NAME and Pyr10; then, hearts and abdominal aorta were collected for further analysis. **(A)** Systolic blood pressure (mmHg) measured non-invasively by tail-cuff in the different groups of mice during the 8-week treatments. **(B)** Western blots and quantifications of p-eNOS and eNOS, respectively, in abdominal aorta, with GAPDH as an internal control ($n=3$). **(C–E)** Heart weight/body weight ratio (mg/g) and echocardiographic left ventricular parameters (IVSTd, LVIDd, and LVPWd in cm; EF and FS in %) and in the different groups of mice after the 8-week treatments. **(F, G)** Representative microphotographs of mouse left ventricular sections stained with either hematoxylin/eosin or Masson's trichrome, respectively, by immunohistochemistry, as well as histograms showing semi-quantitative scores of infiltrating leukocytes per section field and fibrotic areas (%). *Black arrows* show infiltrating leukocytes. Sections are of 4 μm thickness. Two sections were analyzed in each condition in animals. All quantitative data are reported as mean ± SEM. Normal distribution of the values is checked by Shapiro-Wilk test. One-way ANOVA tests are performed for multiple comparisons of values followed by *post hoc* Holm-Sidak tests. Two-way ANOVA tests are performed followed by *post hoc* Holm-Sidak tests for blood pressure measurements. All values with $p<0.05$ are considered significant. $^{*}p<0.01$ *versus* WT; $^{\#}p<0.01$ *versus* WT L-NAME. Unedited gels for **(B)** are presented in Supplementary Figure S10. WT, wild-type. Color images are available online.

relationship has been demonstrated between Nox and TRPC3 in the heart, whereby TRPC3 activates and stabilizes Nox (23). P.E. could affect Nox by inhibiting TRPC3, leading to decreased cytosolic ROS and nucleus DNA damage. Further work using mitochondrial Ca^{2+} and ROS probes might be interesting to dissect the compartmentalized effects of P.E. and TRPC3 inhibition on oxidative stress generation.

All the previously observed anti-proliferative, anti-fibrotic, and anti-oxidative effects were accompanied by calcineurin and NFATc3 inhibition. To further confirm the necessity of this pathway in the effects of P.E., CsA, which inhibits calcineurin-dependent NFATc dephosphorylation and activation, was used and resulted in similar effects. All the observed effects were mediated in a non-cytotoxic manner, and apoptotic gene expression in *CASP3* and *BCL2* remained unchanged. Several studies have demonstrated the effect of polyphenols on apoptosis (5); however, compound concentrations used were high in the micromolar range, which might explain the lack of effect seen in our study. Studies have shown that phenolic compounds possess anti-fibrotic properties (29, 31, 41); however, the high physiologically irrelevant concentrations used *in vitro* dissociate the results from those obtained *in vivo*. Besides, single compounds are often studied, which makes human *in vivo* translation unrealistic since such large quantities cannot be found in a single nutrient nor can be obtained on a daily basis through a balanced diet that usually contains a mixture of phenolic compounds (54). In this study, low nanomolar concentrations were used, which reflect the levels found in tissues in whole organisms (8, 15, 45).

To explain the observed effects of P.E. on NFATc3 activation and CF phenotype, and since NFATc3 is activated by Ca^{2+} (32), we studied basal un-stimulated Ca^{2+}, ROCE stimulated by AngII and SOCE. Basal and AngII-mediated Ca^{2+} entries but not SOCE were inhibited by P.E. treatment. Phenolic compounds such as non-steroidal estrogen diethylstilbestrol and various analogs have been shown to affect SOCE (10); however, these effects were present at 1 and 10 μM concentrations, which are at least 20 times higher, for a single compound, than what is used in our study. Minimal effects were observed with the 100 nM concentrations. Aside from the concentration differences between this study and literature, cell type and Ca^{2+} machinery as well as the use of a mixture of phenolic compounds could play a role in the observed results. Similar to human results, TRPC3 expression was increased by FBS and diminished under P.E., and to further validate the implication of TRPC3 in Ca^{2+} entry and

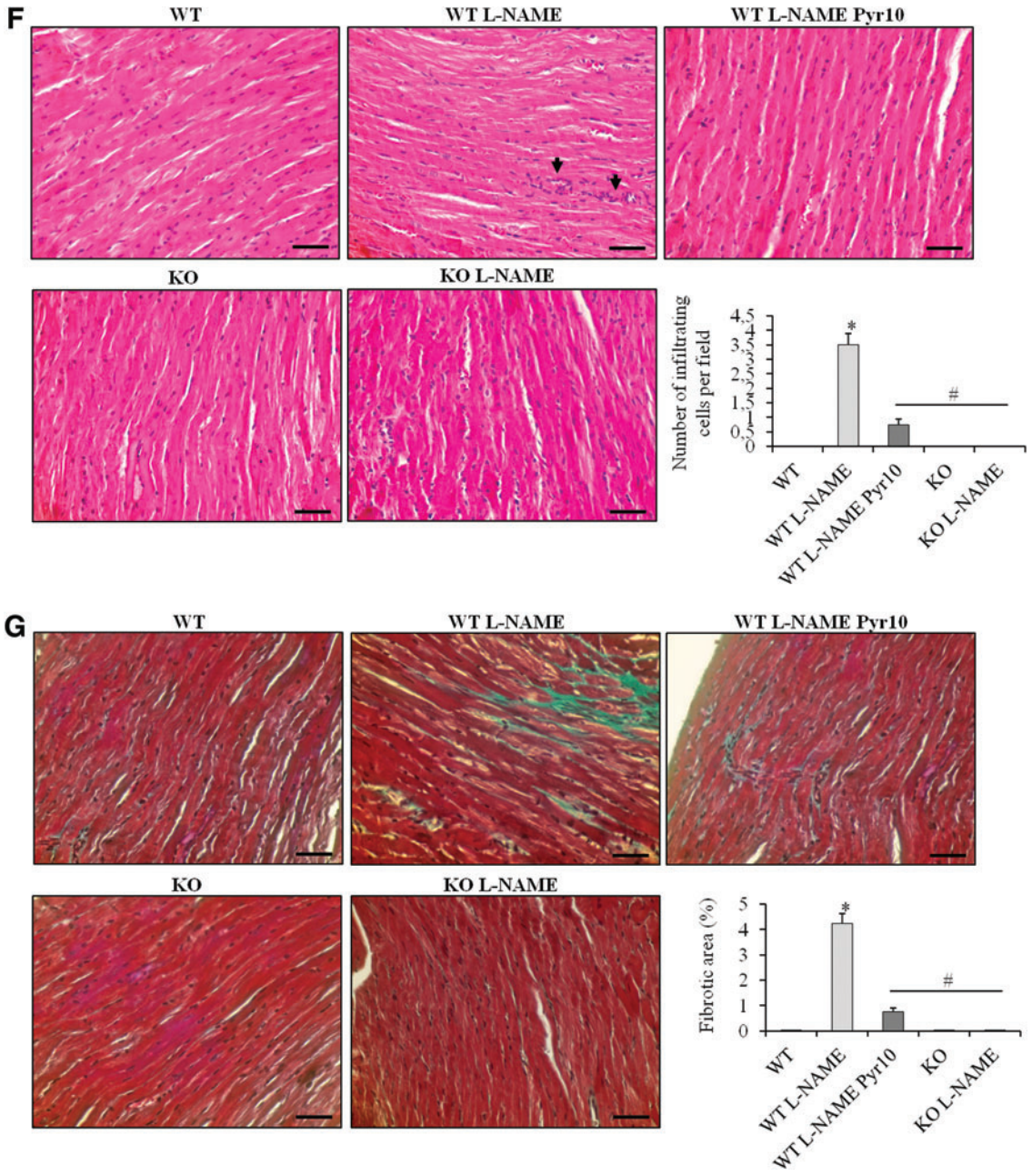

FIG. 7. *(Continued)*

the inhibitory effects of P.E., a specific channel blocker was used, Pyr10. Pyr10 was chosen over the commonly used Pyr3, since the latter has been shown to block ORAI1, a closely related Ca^{2+} channel (55). Pyr10 exhibited the same inhibitory profile as P.E. with decreases in basal Ca^{2+} and ROCE as well as CF proliferation. The effect of Pyr10 on basal Ca^{2+} was lower than the effect on ROCE, suggesting that other Ca^{2+} regulatory proteins might be implicated in Ca^{2+} homeostasis in resting states. A positive feedback loop was also found, whereby Ca^{2+} entering through TRPC3 activates NFATc3, leading to TRPC3 gene transcription and aggravation of the fibrotic phenotype. Similar signaling circuits have been described in cardiomyocytes between TRPC channels and NFAT signaling, exacerbating cardiac remodeling (18, 27). When other non-specific inhibitors of TRPs channels were tested, a further decrease in Ca^{2+} entries was observed, suggesting that other ion channels might be also contributing to ROCE in these cells. However, in this study, blocking TRPC3 was sufficient to significantly alter Ca^{2+} entries, decrease NFATc3 activation, and block all the fibrotic phenotypes. SOCE has been described in CFs from animals and humans (4), but since this pathway was not affected by P.E., we did not look further into its contribution to CF phenotype.

Since the Ca^{2+} inhibitory effects of P.E. were examined in 24-h treatments showing a downregulation of the channel protein expression and NFATc3 activity, P.E. was acutely applied to CFs to isolate the main regulator of the TRPC3-

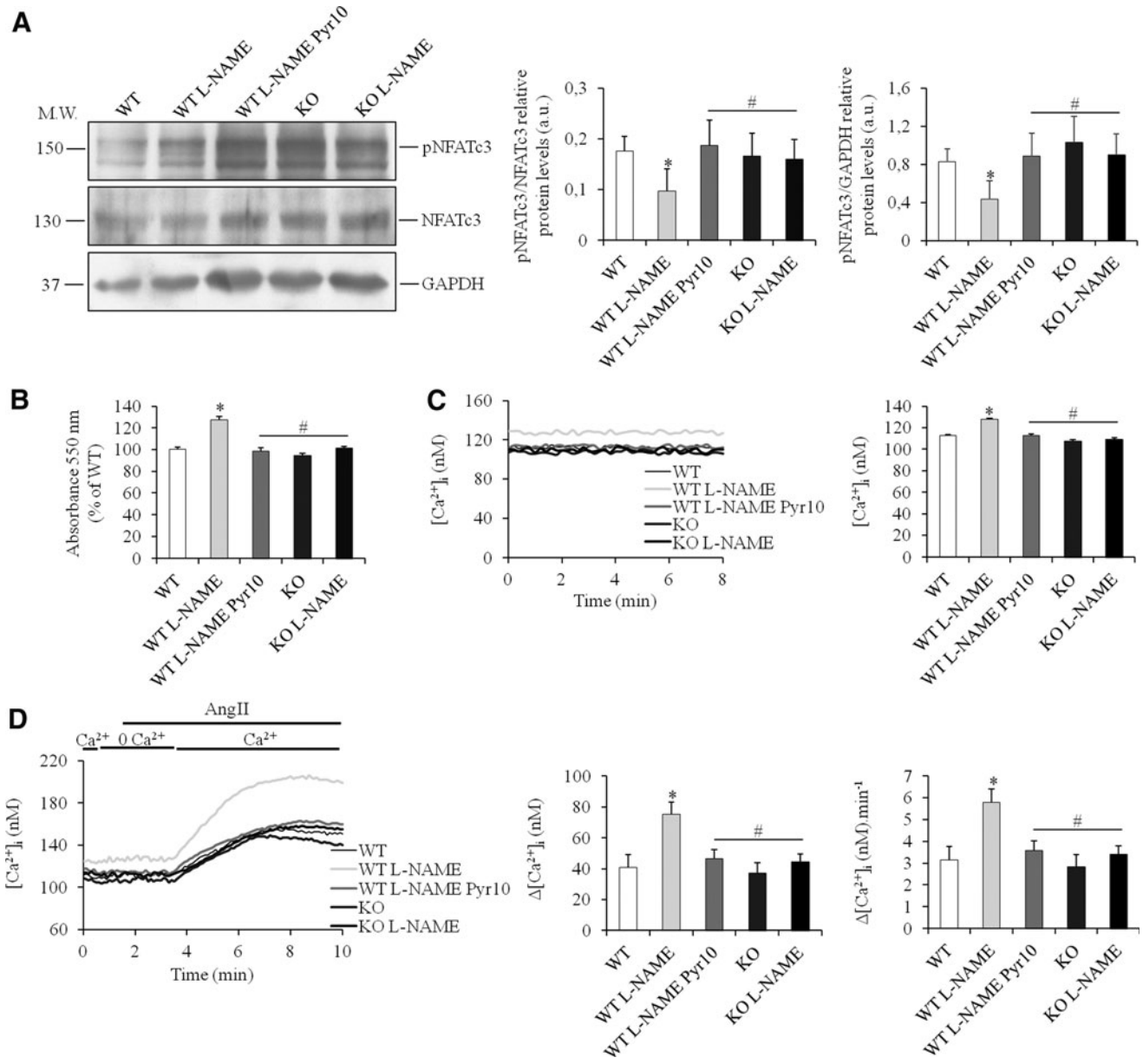

FIG. 8. Pharmacological inhibition and genetic deletion of TRPC3 decreases activation of ventricular CFs *in vivo* in mice. Mice were treated for 8 weeks with L-NAME and Pyr10; then, CFs were isolated for further analysis. **(A)** Western blots and quantifications of pNFATc3 and NFATc3, respectively, in isolated CFs with GAPDH as an internal control ($n = 3$). **(B)** CF proliferation estimated by MTT assay as a percentage of sham; absorbance at 550 nm. **(C, D)** Basal Ca^{2+} and AngII-mediated Ca^{2+} entries (ROCE) and quantifications reported as amplitudes ($\Delta[Ca^{2+}]_i$ [n*M*]) and rates of Ca^{2+} entry ($\Delta[Ca^{2+}]_i$ [n*M*]·min^{-1}) in isolated CFs. All Ca^{2+} imaging data are an average from several cells ($n = 15$ cells) from one coverslip and are representative of several independent recordings ($n = 3$). All quantitative data are reported as mean ± SEM. Normal distribution of the values is checked by Shapiro-Wilk test. One-way ANOVA tests are performed for multiple comparisons of values followed by *post hoc* Holm-Sidak tests. All values with $p < 0.05$ are considered significant. $^{*}p < 0.01$ *versus* WT; $^{\#}p < 0.01$ *versus* WT L-NAME. Unedited gels for **(A)** are presented in Supplementary Figure S10.

NFATc3 loop. After the Ca^{2+} signal reached a plateau, P.E. perifusion resulted in a sudden drop in fluorescence signal, suggesting that the compound might be acting directly on the ion channel. When CFs were pre-incubated for 5 min with P.E., a stronger inhibition was observed, which may pinpoint to other TRPC3 regulatory proteins that might be also affected. Further studies beyond the scope of this work might be interesting to dissect the molecular mechanism by which P.E. act on TRPC3 channels. Pyr10 was also added with P.E. but did not lead to a further inhibition of Ca^{2+} entry, further suggesting that P.E. act on TRPC3. This acute treatment did not affect NFATc3 dephosphorylation, which pinpoints to TRPC3 as the main regulator in the TRPC3-NFATc3 signaling circuit. The absence of effect on NFATc3 is also consistent with NFATc3 dephosphorylation and rephosphorylation kinetics that require several minutes for establishment (64). Recently, it has been

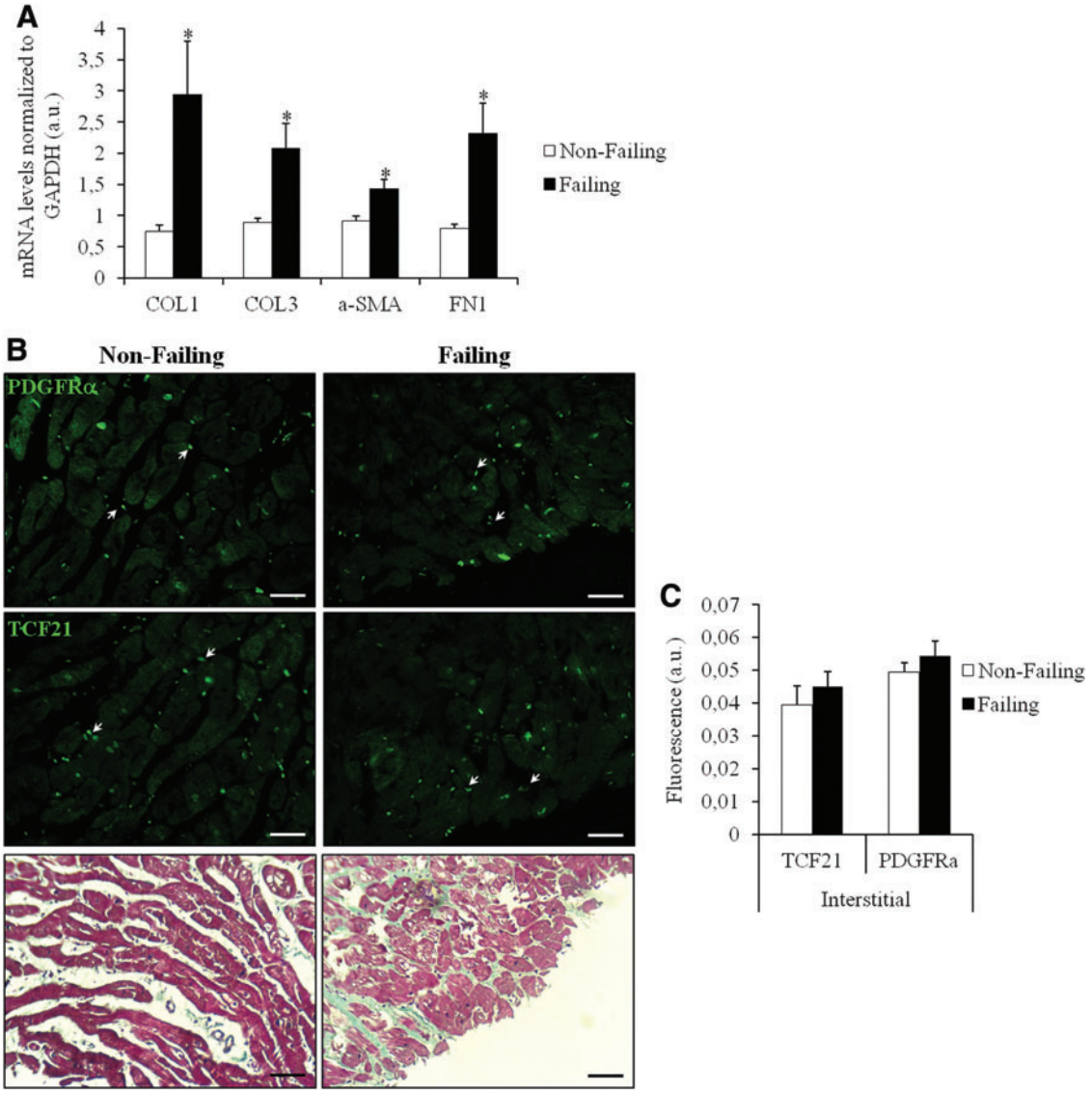

FIG. 9. TRPC3 is present in human ventricular CFs and correlates with MF. (A) Gene expression of myofibroblast and ECM markers (*COL1*, *COL3*, *α-SMA*, and *FN1*) with *GAPDH* as housekeeping gene in human ventricular CFs. **(B, C)** Representative microphotographs and fluorescence quantifications of human left ventricular adjacent serial sections stained with Masson's trichrome and labeled with PDGFRα and TCF21 by immunofluorescence. Magnifications: ×200. Scale bars: 25 μm. ($n=13$). Sections are of 4 μm thickness. **(D)** Representative microphotographs of human left ventricular sections labeled with TRPC3 by immunohistochemistry. Magnifications: ×100 (*left*), ×200 (*right*). Scale bars: 50 μm (*left*), 25 μm (*right*). ($n=13$). Sections are of 4 μm thickness. **(E)** Representative microphotographs and colocalization analysis of human left ventricular sections labeled with TRPC3 and *Col1* by immunofluorescence. Nuclei are stained with DAPI. Magnifications: ×100 and ×400 (zoom in). Scale bars: 50 μm and 12.5 μm (zoom in). ($n=13$). Sections are of 4 μm thickness. **(F)** Western blots of TRPC3 and COL1 in human ventricular CFs with GAPDH as an internal control and correlation between the two proteins ($n=13$). **(G)** Correlation between TRPC3 expression in human ventricular CFs and AngII-mediated Ca^{2+} entry (ROCE) in these cells ($\Delta[Ca^{2+}]_i$ [n*M*]). All Ca^{2+} imaging data are an average from several cells ($n=15$ cells) from one coverslip and are representative of several independent recordings ($n=3$). Pearson correlation coefficient is used to measure the strength of the relationship between TRPC3/COL1 and TRPC3/$\Delta[Ca^{2+}]_i$. All quantitative data are reported as mean ± SEM. Normal distribution of the values is checked by Shapiro-Wilk test. One-way ANOVA tests are performed for multiple comparisons of values followed by *post hoc* Holm-Sidak tests. All values with $p<0.05$ are considered significant. *$p<0.01$ *versus* non-failing. Unedited gels for **(F)** are presented in Supplementary Figure S11. *COL3*, collagen 3; PDGFRα, platelet-derived growth factor receptor alpha; TCF21, transcription factor 21. Color images are available online.

shown that inhibition of TRPC3 attenuates TGF-β1-induced myofibroblast differentiation of neonatal rat CFs through Nox isoform 2 (Nox2) dependent RhoGEF-H1 activation (39). TRPC3 interacts with Nox2, thereby protecting it from proteasome-dependent degradation and amplifying its activity whereas Nox2 stabilizes TRPC3 and also enhances its activity (23). Besides, NFATc3 activation in CFs by AngII was mediated by ROS (14). This raises the question as to whether possible Nox2 activity modulation by P.E. might be contributing to the observed effects on CFs. However, the

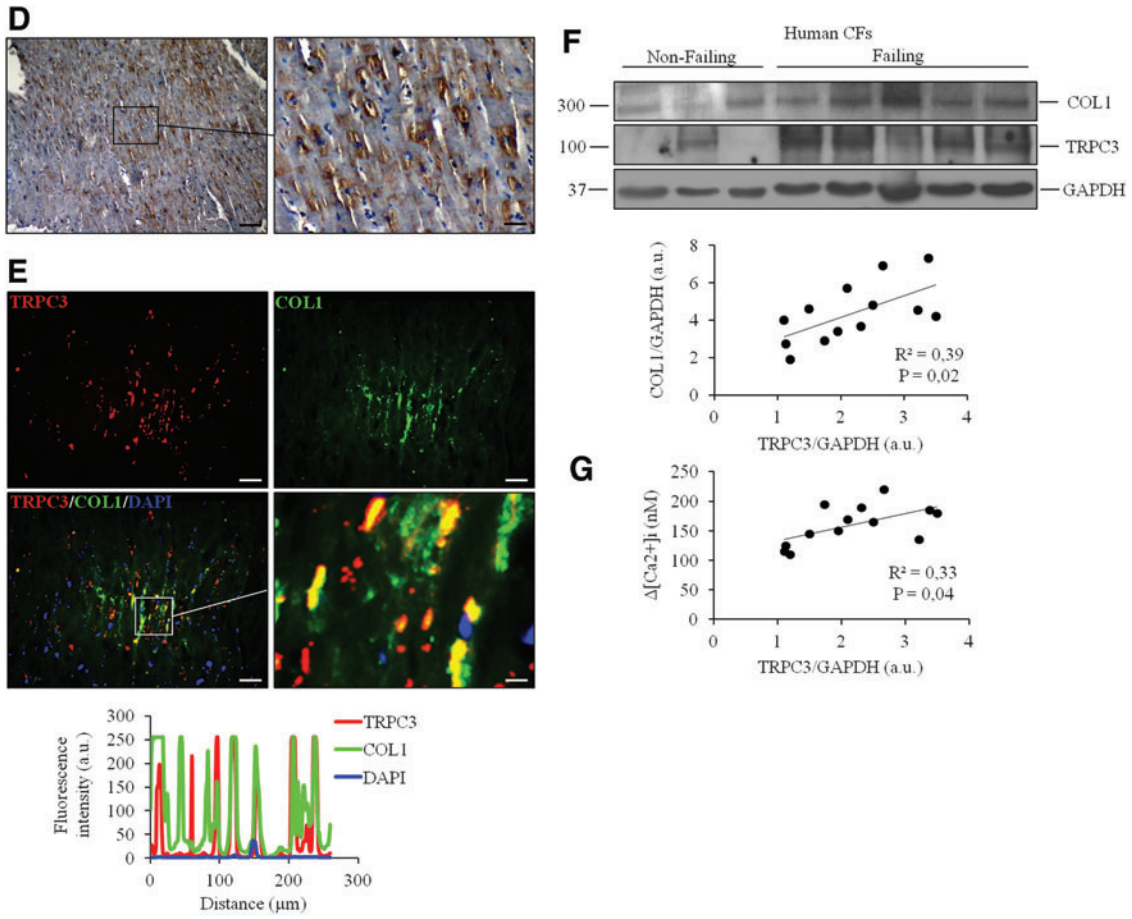

FIG. 9. *(Continued)*

acute effects of P.E. on Ca^{2+} entries *via* TRPC3 as well as the similar effects of Pyr10, which is a direct inhibitor of TRPC3, on the CF phenotype, support a major role for TRPC3 in mediating the fibrotic response of CFs. In addition, AngII stimulation induced nuclear localization of NFATc3 in an ROS independent manner (14). These results indicate not only that TRPC3-mediated Ca^{2+} and ROS pathways act synergistically and concurrently but also that each pathway is sufficient to drive the fibrotic response of CFs.

Most animal models of heart disease culminate in cardiac hypertrophy or failure with or without interstitial fibrosis. Based on this, we chose the L-NAME model of cardiac fibrosis with the absence of hypertrophy (22). L-NAME was also used to blunt the blood pressure-lowering effects of P.E., as previously described (46), and thus test the direct blood pressure-independent effects of P.E. on MF. This hypertensive model induced cardiac perivascular, sub-epicardial, and interstitial fibrosis, with extensive PDGFRα and TCF21-positive cells, indicating increased epicardial cell recruitment to the myocardium. Similar cardiac fibrotic patterns have been described in angII-induced hypertension (1) with expansion of resident CF lineages (1, 20, 35, 36). P.E. did not affect blood pressure elevation induced by L-NAME nor did it increase eNOS phosphorylation levels in blood vessels. Despite the lack of effects on blood pressure, cardioprotective effects of P.E. were observed with a significant amelioration in left ventricular function and cardiac stress markers, abrogation in MF and epicardial cell recruitment, as well as inflammation. Similar blood pressure-independent effects on heart were described in the spontaneously hypertensive rat (62, 63). When ventricular CFs were isolated from hypertensive rats, cells from L-NAME hearts presented a higher proliferation rate, fibrotic secretions, oxidative stress, and TRPC3-NFATc3 activation. P.E.-treated hearts presented with CFs of a less fibrotic phenotype. The $2\,mg\cdot kg^{-1}$ dose used in this study corresponds to a total of 22.68 mg P.E. for an adult of 70 kg. Since a typical glass of red wine contains 100 mg of polyphenols (60), the dose in our study represents a feasible daily consumption of polyphenols as a mixture in a matrix of food. A recent review of the literature showed that most of the studies on polyphenols and cardiac fibrosis used daily doses of at least $5\,mg\cdot kg^{-1}$ of single compounds, which is difficult to obtain as a daily consumption of polyphenol-rich diets alone. Besides, polyphenols as a mixture have shown improved efficacy and consistent results in cardiovascular disease prevention (12) as compared with single compounds (51, 60).

The importance of TRPC3 in the development of MF was further examined by the use of specific pharmacological blockade through Pyr10 and TRPC3 ablation in mice made hypertensive with L-NAME administration. Similar to rats, TRPC3 blockade ameliorated cardiac function and decreased MF and inflammation. Thus, the presence of TRPC3 seems to

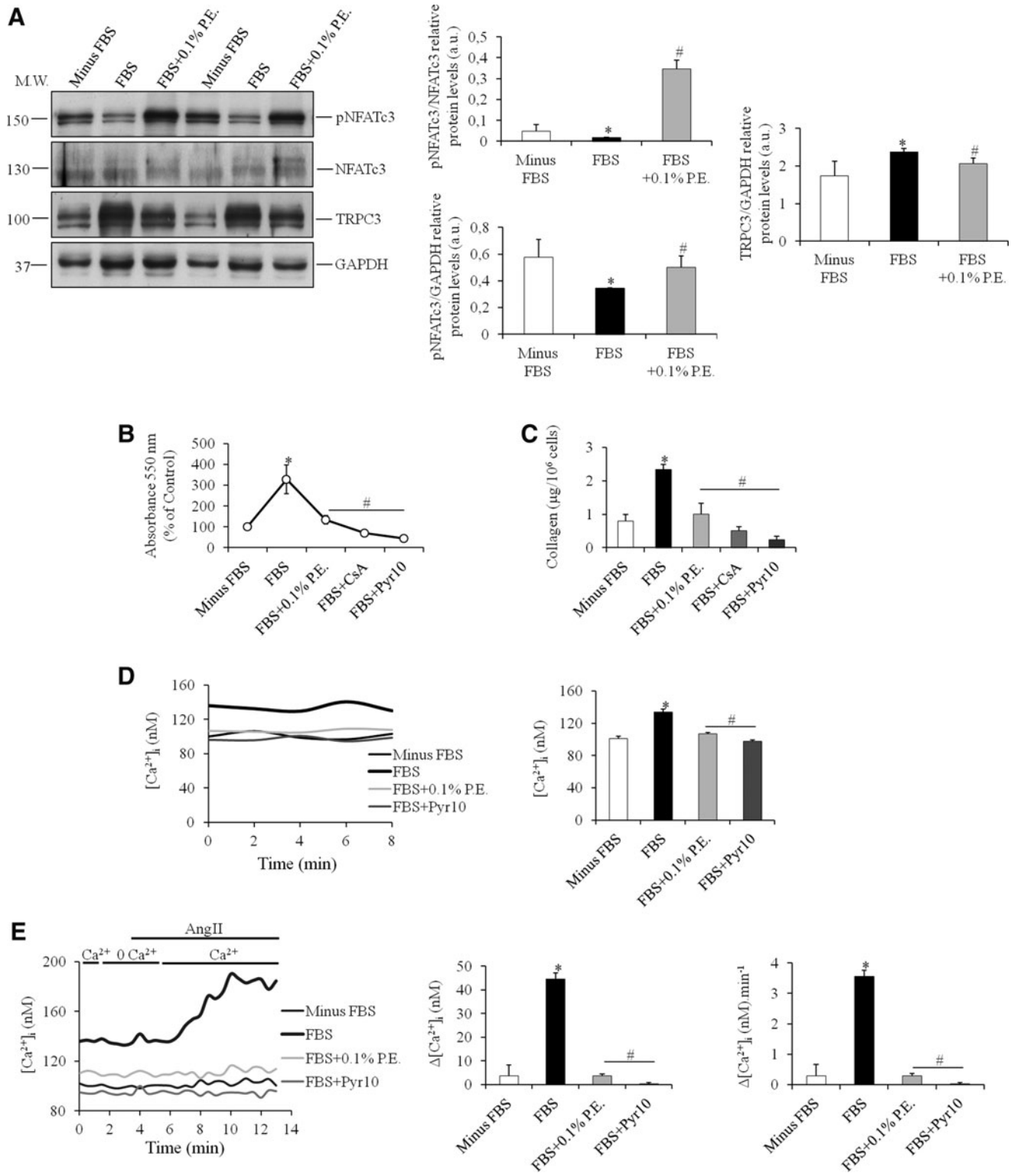

FIG. 10. TRPC3-NFATc3 inhibition decreases proliferation and collagen secretion of human ventricular CFs. Human CFs were cultured for 3 days in the presence of 10% FBS; then, they were serum starved for 1 day before treating them for an additional 1 day with 10% FBS either alone or with 0.1% P.E., Pyr10, and CsA whereas control cells remained without serum. **(A)** Western blots and quantifications of pNFATc3, NFATc3, and TRPC3 in cultured human ventricular CFs with GAPDH as an internal control ($n=3$). **(B)** CF proliferation estimated by MTT assay as a percentage of control; absorbance at 550 nm. **(C)** Collagen synthesis by CFs measured by sircol assay and reported as $\mu g/10^6$ cells. **(D)** Basal Ca^{2+} traces and quantifications in human ventricular CFs. **(E)** AngII-mediated Ca^{2+} entry (ROCE) traces and quantifications reported as amplitudes ($\Delta[Ca^{2+}]_i$ [n*M*]) and rates of Ca^{2+} entry ($\Delta[Ca^{2+}]_i$ [n*M*[$\cdot min^{-1}$) in human ventricular CFs. All Ca^{2+} imaging data are an average from several cells ($n=15$ cells) from one coverslip and are representative of several independent recordings ($n=3$). All quantitative data are reported as mean ± SEM. Normal distribution of the values is checked by Shapiro-Wilk test. One-way ANOVA tests are performed for multiple comparisons of values followed by *post hoc* Holm-Sidak tests. All values with $p<0.05$ are considered significant. $^{*}p<0.05$ *versus* Control; $^{\#}p<0.05$ *versus* FBS. Unedited gels for **(A)** are presented in Supplementary Figure S11.

be essential for not only the induction of fibrosis in the different heart regions but also the epicardial reactivation of CF developmental programs in response to cardiac injury and remodeling. In other pressure-overload models, TRPC3 inhibition, either alone or combined to TRPC6, has been shown to possess cardiac anti-fibrotic properties (39, 58).

Intriguingly, blood pressure in Pyr10 and TRPC3$^{-/-}$ animals treated with L-NAME was similar to controls, despite the channel implication in endothelial cell function and vasoconstriction as well as its link to elevated blood pressure in animals and humans (9, 44). Other studies showed that TRPC3 has a fundamental role in endothelium-derived hyperpolarization-mediated vasodilation and thus in the regulation of vascular tone (57); hence, the channel seems to contribute to the balance between vasoconstriction and vasodilation. Since TRPC3 has been also linked to nitric oxide production (19) and L-NAME acts by blocking the same pathway, a competitive action between the two might explain the blood pressure results in our study. When ventricular CFs were isolated from the different treated groups of mice, cells from L-NAME hearts presented a higher proliferation rate and TRPC3-NFATc3 activation whereas TRPC3 pharmacological and genetic inhibition resulted in a blunted fibrotic phenotype.

Growing evidence supports the role of TRPC3 in cardiovascular disease; however, therapeutic targeting has been hindered by a lack of selective inhibitors. YM58483 and SKF96365 target multiple TRPC and SOCE channels as well as T-type Ca^{2+} channels (59, 74); whereas Pyr3, the first reported selective TRPC3 blocker, also inhibits ORAI1 at concentrations similar to those for TRPC3 (55). The pyrazole compound used here, Pyr10, might pave the way for enhancing basic studies of these channels in native tissues and for the development of novel therapeutic strategies.

Remarkably, TRPC3$^{-/-}$ mice presented a completely blunted MF despite the elevated blood pressure for more than 6 weeks. This gene knockout model was global, which is some sort of limitation, since the relative contribution of cardiomyocytes, CFs, and smooth muscle cells cannot be distinguished; however, all our *in vitro* data support relevance in CFs. Besides, we employed a hypertensive model that develops MF without cardiac hypertrophy, possibly limiting the implication of cardiomyocytes in the development of this pathology. Since all progress in heart disease management lay in either systemic non-targeted non-cell-specific pharmacological treatments or device-based therapies, these global knockout models are relevant.

In conclusion, we demonstrate a direct modulation of TRPC3 channels and NFATc3 signaling in rat ventricular CFs by physiologically relevant low concentrations of polyphenols as well as specific channel inhibitor Pyr10 (Supplementary Fig. S7); this modulation abrogates the fibrotic phenotype of fibroblasts. We then show that modulating TRPC3-NFATc3 *in vivo* in ventricular CFs either by polyphenols in L-NAME hypertensive rats or by specific pharmacological inhibition and genetic deletion (TRPC3$^{-/-}$) in L-NAME hypertensive mice ameliorates MF in a blood pressure-independent way. Finally, we provide the first evidence that functional TRPC3 is present in human ventricular CFs, activates NFATc3, and is associated to MF. TRPC3 modulation by polyphenols or targeted therapy might constitute an interesting therapeutic approach for MF management.

Materials and Methods

Animals

This study was approved by the Ethical Committee of Saint Joseph University. Protocols were designed according to the Guiding Principles in the Care and Use of Animals approved by the Council of the American Physiological Society and were in adherence to the Guide for the Care and Use of Laboratory Animals published by the US National Institutes of Health (NIH Publication No. 85-23, revised 1996) and according to the European Parliament Directive 2010/63 EU.

The study was conducted in 8- to 10-week-old male Wistar rats and male TRPC3 knockout (TRPC3$^{-/-}$) mice with their age-matched littermate WT controls. Rats were obtained from the ''Centre d'Elevage R. Janvier'' (Le Genest-Saint Isle, France); whereas mice were developed at the Comparative Medicine Branch of the NIEHS on a 129SvEv/C57BL/6J mixed background by deleting exon 7 of the *Trpc3* gene in a three-step process (16), and they were obtained from Pr Nancy Rusch's laboratory stock at the University of Arkansas for Medical Sciences. Animals were housed at a stable temperature (25°C) and humidity (50% ± 5%), and they were exposed to a 12:12 h light-dark cycle. They were fed ordinary rodent chow, had free access to tap water, and were acclimatized for at least 1 week under these conditions before the start of the study.

Rat, mouse, and human fibroblast isolation

Ventricular CFs were isolated from rats and mice and maintained in primary culture. Briefly, animals were anesthetized by ketamine (75 mg·kg^{-1}; Interchemie, Waalre, Holland) and xylazine (10 mg·kg^{-1}; RotexMedica, Trittau, Germany). Pedal withdrawal reflex was performed to ensure adequate depth of anesthesia; when animals were completely non-responsive to toe pinching, their hearts were quickly removed and transferred to modified Tyrode solution, containing (in m*M*): 117 NaCl; 5.7 KCl; 1.7 $MgCl_2$; 4.4 $NaHCO_3$; 1.5 KH_2PO_4; 10 HEPES; 10 creatine monohydrate; 20 taurine; 11.7 D-glucose; 1% bovine serum albumin (BSA); and pH 7.1 with NaOH. Ventricles were dissected and then digested by two successive modified Tyrode enzymatic baths: 20 min with collagenase type V (165.1 U·mL^{-1}) and protease type XXIV (4.62 U·mL^{-1}; Sigma-Aldrich, St. Louis, MO), and then 20 min with collagenase type V (157 U·mL^{-1}).

Cardiomyocytes were discarded after a first centrifugation (500 rpm, 10 min); then, fibroblasts were collected after the second one (2000 rpm, 10 min) and resuspended in Dulbecco's modified Eagle's medium (DMEM) containing 10% FBS (Lonza, Basel, Switzerland) and 1% penicillin/streptomycin. After 4 h of culture, the non-adherent cells were removed and the medium was replenished. Fibroblast counting was done with a hemocytometer to ensure that the same number of cells was studied in each condition. After 24 h of culture, all cells had the fibroblast characteristic elongated fusiform and in spindle shape.

For all the *in vitro* studies and since CFs lose their phenotype in long-term cultures (53), treatments were conducted on 3-day cultured cells without any passage to ensure cells retained their original phenotype. Three cultures were conducted for each condition. For the *in vivo* studies, CFs isolated from sham and L-NAME rats with or without P.E. were grown for just 3 days and further biochemical and molecular experiments were conducted.

Human ventricular CFs were obtained from failing and non-failing hearts of patients undergoing valve replacement surgery ($n = 13$ patients). Clinical data of the patients are presented in Supplementary Table S1. The study was approved by the Ethical Committee of Saint Joseph University. All subjects gave informed consent. Ventricular tissues were dissected and washed in modified Tyrode; then, CFs were isolated and cultured as previously described.

Extract of grape pomace polyphenols

The grape pomace byproducts used are the solid remains of grapes (Cabernet Sauvignon, Marselan, and Syrah) obtained in wine industries after the pressing step. It contains the skins, pulp, seeds, and stems of the fruit. Extraction and quantification of the P.E. were conducted as previously described (3) with a slight modification. Briefly, byproducts were ground; then, a heat solid/liquid extraction process with 70% ethanol/water was performed at a ratio of 1:2 (w/v) with agitation. Total P.E. contained in the extract were quantified by using the conventional Folin-Ciocalteu colorimetric assay against a standard curve of gallic acid. P.E. accounted for 92% of the final extract with 8% residual sugars and fibers.

Phenolic standards for high-performance liquid chromatography (HPLC) were the most commonly described in literature: gallic acid, protocatechin, hydroxybenzoic acid, catechin, epigallocatechin, caffeic acid, chlorogenic acid, epicatechin, p-coumaric acid, gallo-catechin gallate, ferulic acid, resveratrol, cinnamic acid, rutin, myricetin, quercetin, and kaempferol (Sigma-Aldrich). HPLC with diode-array detection analyses were carried out with a HPLC system (Waters Alliance, Milford, MA) equipped with a quaternary Waters e2695 pump. In addition to an ultraviolet-visible (UV-vis) photodiode array spectrophotometer (250–700 nm) Waters 2998, a fluorescence detector (excitation 330/emission 374 nm) was used with the control system and data collection Empower 3 software. P.E. separation was realized on a Discovery C18, 5 μm, 250 × 4.6 mm, column (Supelco, Bellefonte, Pennsylvania) with a C18, Supelguard Discovery 18, 20 × 4 mm, 5 μm precolumn (Supelco) at 30°C. Chemical characterization is presented in Table 1.

In vitro *treatments*

After isolation, CFs were kept for 3 days in culture by using complete medium with 10% FBS. Cell cycle synchronization was then conducted by serum starvation (0.5%) for 24 h as previously described (41); then, the different treatments were applied for an additional 24 h. Overall, 10% FBS was present in all conditions except for the control cells. Cells were treated with different concentrations of P.E. corresponding to 0.01%, 0.05%, and 0.1% dilutions of the stock P.E. solution (Table 1), Pyr10 dissolved in dimethylsulfoxide (DMSO), or 1 μM CsA dissolved in water. Pyr10 was chosen since it possesses higher specificity for TRPC3 than TRPC6 and ORAI1 channels, as compared with other pyrazole compounds (55).

Animal groups and in vivo *treatments*

Since most animal models of heart disease present in cardiac hypertrophy or failure with or without interstitial fibrosis, we chose the well-described L-NAME model of cardiac fibrosis with the absence of hypertrophy (22). Besides, we used L-NAME to blunt the blood pressure-lowering effects of P.E., as previously described (46), and thus test the direct blood pressure-independent effects of P.E. on MF.

Rats were randomly divided into four groups ($n = 8$ in each group): Sham, Sham P.E., L-NAME, and L-NAME P.E. L-NAME was given at a dose of 50 $mg \cdot kg^{-1}$ per day, whereas P.E. was given at a dose of 2 $mg \cdot kg^{-1}$ per day to achieve a low-dose regimen of each phenolic compound *in vivo* (Table 1). Substances were given in tap water for 8 weeks. To make sure that each animal received the complete dose of L-NAME and P.E., the calculated amount was given to each rat in the appropriate volume of water. Daily water consumption was estimated individually for every animal 1 week before the experiment. During the experiment, water consumption was controlled and L-NAME and P.E. concentrations in the drinking fluid were adjusted accordingly.

Mice were randomly divided into five groups ($n = 6$ in each group): WT, WT L-NAME, WT L-NAME Pyr10, KO, and KO L-NAME. L-NAME was administered as in rats. Pyr10 was delivered by osmotic minipumps (Alzet, Durect, CA) that were placed subcutaneously on the back slightly posterior to the scapulae at a dose of 0.1 $mg \cdot kg^{-1}$ per day as described for other similar pyrazole compounds (24). Protocol duration was also 8 weeks.

Echocardiography and blood pressure measurement

Echocardiography was performed with a Sonoscape S2V imaging system and a 9-MHz C611 transducer, which is designed specifically for mice and rats. After the 8-week treatments and just before sacrifice, rats and mice were anesthetized with isoflurane (3% for introduction and 1.5% during imaging). Hearts were viewed in the short axis between the two papillary muscles and analyzed in M-mode. Parameters included: IVSTd, LVIDd, LVPWd, EF, and FS.

Systolic blood pressure was measured by using the non-invasive tail-cuff method (IITC), and animals were trained for 2 weeks before the study to acclimatize. Briefly, awake rats and mice were placed in acrylic holders for 10 min before taking the measurements. To avoid variations in blood pressure due to day cycle, all measurements were carried out between 10 a.m. and noon and all measurements were taken in duplicates at each condition.

Ca^{2+} imaging

CFs grown for 3 days on glass coverslips were incubated for 45 min in serum-free DMEM containing 4 μM fluo4-am (Molecular Probes, ThermoFisher Scientific) dissolved in DMSO. Fluo-4 was chosen since some polyphenols were shown to interfere with fura-2 (25). Cells were washed twice in standard HEPES buffered saline solution (HBSS) containing (in mM): 135 NaCl; 4 KCl; 1.8 $CaCl_2$; 1 $MgCl_2$; 2.5 HEPES; 10 glucose; and pH 7.4 with NaOH. As previously described (52), since TRPC3 are ROCE channels physiologically activated by DAG, two perfusion protocols were performed by using either DAG analog (OAG) (100 μM) or Ang II (100 nM) (Sigma-Aldrich) to study ROCE. Nifedipine (1 μM) was used to inhibit L-type Ca^{2+} channels. Pyr10 was added at a concentration of 10 μM. The non-selective TRPCs blockers SKF96365 (30 μM), gadolinium Gd^{3+} (100 μM), and YM58483 (1 μM) were from Sigma. SKF06365 and Gd^{3+} were diluted in ultrapure water, whereas YM58483 was dissolved in DMSO. Cells were incubated with the different

Table 1. Chemical Characterization of Grape Pomace Polyphenols

	Extract content (mg/L)	In vitro *concentration, nM (0.01%, 0.05%, and 0.1% P.E. dilution, respectively)*	In vivo *daily intake (μg/kg body weight)*
Gallic acid	3.2	1.88/9.4/18.8	21
Hydroxybenzoic acid	18.6	13.47/67.35/134.7	124
Catechin	0.8	0.27/1.35/2.7	5.33
Epigallocatechin	21.4	6.99/34.95/69.9	144
Chlorogenic acid	5.3	1.5/7.5/15	35.33
p-Coumaric acid	2.6	1.58/7.9/15.8	17.33
Gallocatechin gallate	4.7	1.02/5.1/10.2	31.33
Ferulic acid	6.9	3.55/17.75/35.5	46
Resveratrol	9.8	4.29/21.45/42.9	65.33
Rutin	23.6	3.87/19.35/38.7	157.33
Myricetin	24.1	7.57/37.85/75.7	160.66
Quercetin	15.4	5.09/25.45/50.9	102.66
Kampferol	17.6	6.15/30.75/61.5	117.33

P.E. was diluted in cell culture medium to corresponding factors, 1/10,000 or 0.01%, 1/2000 or 0.05%, and 1/1000 or 0.1%.
P.E., extract of grape pomace polyphenol.

inhibitors from the start till the end of the recordings. P.E. and Pyr10 were also acutely added after Ca^{2+} entries. On and off Ca^{2+} perfusion was performed as a leak control. To measure basal un-stimulated Ca^{2+} level, cell monitoring in the presence of extracellular Ca^{2+} was performed for several minutes. Since SOCE was also described in CFs (4), we also studied the effects of P.E. on cells incubated with CPA, which is a sarco-endoplasmic reticulum Ca^{2+} ATP-ase inhibitor that depletes the endoplasmic reticulum Ca^{2+} stores and activates SOCE. Grape pomace P.E. contained tannins such as gallic acid that combines various metal cations (21); therefore, the presence of interaction between tannins and Ca^{2+} ions was tested by acutely adding gallic acid (Sigma-Aldrich) with the same concentration as found in the grape pomace P.E. (18.8 n*M*) on CFs. Ionomycin (2 μM) and ethylene glycol tetraacetic acid (EGTA 10 m*M*) were consecutively added at the end of the perfusion protocols to check for the maximum and minimum fluorescence values.

Intracellular Ca^{2+} concentration ($[Ca^{2+}]i$) was estimated by Tsien's formula $[Ca^{2+}]i = K_D$ $([F - F_{min}])/([F_{max} - F])$. The dissociation constant for Ca^{2+} binding, K_D, was estimated to be 345 n*M*. Fluorescence experiments were carried out at room temperature. Ca^{2+} entry amplitudes ($\Delta[Ca^{2+}]_i$ [n*M*]) were measured by subtracting the ratio values as well as intracellular Ca^{2+} values just before re-adding Ca^{2+} from those at the Ca^{2+} peak. The rates of Ca^{2+} entry ($\Delta[Ca^{2+}]_i$ (n*M*)$\cdot$min^{-1}) were estimated by the slope of increasing fluo-4 fluorescence after the re-addition of Ca^{2+}, calculated between time points corresponding to a 10% and a 90% variation in fluo-4 values (relative to the maximal 100% variation). Fluorescence images of several cells were recorded and analyzed with a digital fluorescence imaging system (InCyt Im2; Intracellular Imaging, Inc., Cincinnati, OH). All figures depicting Ca^{2+} imaging traces are an average from several cells ($n = 15$ cells) from one coverslip and are representative of several independent recordings ($n = 3$). Ca^{2+} quantification data are represented as mean ± standard error of the mean (SEM) in bar graphs.

Cell proliferation, migration, viability, and apoptosis assays

Cell proliferation assay was done by using MTT (Bio Basic, Inc., Markham, Canada). After cell culture treatments, the medium was removed and 0.5 mg$\cdot$mL^{-1} MTT water solution was added onto the cells. After 4 h of incubation at 37°C, MTT solution was discarded; then, cells were washed with phosphate-buffered saline (PBS). The MTT formazan purple crystals were then dissolved with 100 μL of 100% DMSO, and absorbance was read at 550 nm.

Scratch wound-healing assay was used to assess cell migration. The cell monolayer was gently and slowly scratched with a sterile 1 mL pipette tip across the center of the well. After scratching, the medium was removed to get rid of detached cells and replenished. Cells were grown for an additional 48 h, and migrating cells were counted.

Cell viability was assessed by trypan blue exclusion test, whereas apoptosis was assessed by propidium iodide staining. After *in vitro* treatments, cells were labeled with trypan blue (0.4% in PBS; Sigma-Aldrich). Trypan blue positive and negative cells were calculated with a hemocytometer. Trypan blue negative cells were regarded as viable. The percentage of viable cells was calculated by using the following formula: total viable cells (unstained)/total cells (stained and unstained) $\times$ 100. Cells were also stained with propidium iodide (3 μM in cell culture medium), and fluorescence was detected at 620 nm.

Enzyme-linked immunosorbent assay, oxidative stress measurement, and sircol collagen and calcineurin assays

Enzyme-linked immunosorbent assay (ELISA) technique was used for quantifying secreted cytokines in plasma and from cell cultures. TGF-β1, IL1, TNF-α, CRP, TnT, and BNP ELISA kits were used according to the manufacturer's protocols (Abcam, Cambridge, United Kingdom).

ROS were measured by using the cell-permeant fluorescent dye 2′,7′-dichlorodihydrofluorescein diacetate (H_2DCF-DA; Molecular Probes, ThermoFisher Scientific). In the presence of peroxides, H_2DCF is converted into the highly fluorescent DCF. Cells were loaded with 20 μM H_2DCF-DA in modified Tyrode for 15 min at 37°C in the dark. After washing, ROS were detected as a result of the oxidation of H_2DCF and fluorescence (ex 488 nm; em 515 nm) was followed with a Nikon eclipse Ts100f fluorescence microscope

equipped with a CCD camera (Basler SCA 640-74, Ahrensburg, Germany).

RNA/DNA damage assay was conducted by using immunofluorescence on CFs with an antibody that recognizes 8-hydroxy-2′-deoxyguanosine, 8-oxo7,8-dihydroguanine, and 8-oxo-7,8-dihydroguanosine (8-OHDG; Abcam), as detailed later in the Immunofluorescence and histopathology section.

Collagen synthesis by fibroblasts was evaluated by the sircol collagen assay (Biocolor, County Antrim, United Kingdom), as previously described (52). Briefly, after cell treatments, the supernatant was collected. Sircol dye reagent was added to each sample and standard. After centrifugation, the collagen-dye pellet was washed and then dissolved with an alkali reagent. Absorbance was read at 550 nm.

Cellular calcineurin phosphatase activity assay kit (Abcam) was used to assay calcineurin (PP2B) activity in rat ventricular CFs according to the manufacturer's protocol. Briefly, the RII phosphopeptide substrate is used as an efficient peptide substrate for calcineurin. The detection of free phosphate released is based on the classic Malachite green assay, and absorbance is read at 620 nm. A series of control conditions is used for each sample to discriminate between the contribution of calcineurin and other phosphatases. Calcineurin requires calcium for its activity, thus the EGTA control sample represents total phosphatase activity less calcineurin. Okadaic acid at 100 and 500 n*M* is known to completely inhibit PP1 and PP2A, whereas it has no effect on calcineurin. Finally, okadaic acid+EGTA inhibits PP1, PP2A, and PP2B, but not PP2C. The analysis of these control conditions for each sample allows the quantification of calcineurin (PP2B) activity in the cellular extract.

Mitochondria extraction

Rat ventricular CFs were cultured and treated; then, mitochondria were isolated as previously described (43). Briefly, cells were trypsinized and washed with cold STE buffer containing the following (in m*M*): 250 sucrose; 5 TRIS; 2 EGTA; and pH 7.4 with HCl. Cells were then resuspended with cold STE containing protease inhibitors and 0.5% fatty-acid-free BSA and transferred to a glass-teflon homogenizer. After 10 slow passes of the tight plunger, the homogenate was spun at 3000 rpm for 3 min at 4°C. The supernatant was then spun at 10,000 rpm for 11 min at 4°C, and the mitochondrial pellet was resuspended with cold STE. Protein concentration was determined by using the Bradford protein assay (Bio-Rad, Marnes-la-Coquette, France). Cytochrome c oxidase subunit 4 (COX4) was used as a mitochondrial protein control.

Western blot

Proteins were extracted from CFs and abdominal aorta (for eNOS studies) by using RIPA buffer with protease and phosphatase inhibitors. Protein concentration was determined by using the Bradford protein assay (Bio-Rad). Proteins were separated by sodium dodecyl sulfate (SDS) 10% polyacrylamide gel electrophoresis (PAGE) and then blotted on Hybond-C membranes (Amersham Biosciences, GE Healthcare). Membranes were blocked with either 5% nonfat milk or 5% BSA and incubated with the various antibodies: eNOS (1/1000; Santa Cruz Biotechnology, Dallas, TX), phospho-eNOS (p-eNOS; Ser1177; 1/1000; Cell Signaling Technology), COL1, NFATc3, phospho-Ser165 NFATc3 (pNFATc3), rat TRPC3, glyceraldehyde-3-phosphate dehydrogenase (GAPDH), COX4 (1/500 for all; Abcam), and mouse TRPC3 clone 10H6 (1/1000; Millipore, Merck). TRPC3 and phospho-Ser165 NFATc3 antibodies were used as previously described (13, 30). Visualization was done by using enhanced chemiluminescence and developed on Kodak films. Three Western blots were performed for each protein and condition.

Immunofluorescence and histopathology

Formalin-fixed human cardiac biopsies as well as rat and mouse hearts were embedded in paraffin, and sections of 4-μm thickness were cut. Rat, mouse, and human paraffin-embedded sections were stained with either hematoxylin/eosin or Masson's trichrome (Sigma-Aldrich) for histopathological evaluation. After staining, sections were rinsed in distilled water, dehydrated in ethanol/water baths with decreasing water content, and finally rinsed in xylene before being mounted with a permanent mounting medium. Rat sections were also stained with α-SMA (BioGenex) by using peroxidase-conjugated secondary antibody followed by DAB staining. Human sections were stained with TRPC3 (Millipore, Merck) followed by DAB staining. Double immunofluorescence was conducted on human sections by using TRPC3 and COL1; nuclei were stained with DAPI.

Further, serial adjacent cardiac sections from rats, mice, and humans were stained with Masson's trichrome and labeled with PDGFRα and TCF21, two known epicardial progenitor transcription factors expressed in resident CFs before and after heart injury. Sections were carried in series to ensure that Masson's trichrome and PDGFRα/TCF21 immunolabeling were conducted in the same heart location and depth, allowing for a delicate analysis of MF and CFs populations; PDGFRα and TCF21 were from Abcam. Cultured rat CFs were fixed with ice-cold ethanol, followed by triton permeabilization and saturation with goat serum and BSA. Cells were then co-stained with 8-OHDG and DAPI. To assess the purity of the cultured cells, immunofluorescence was also performed by using the following antibodies: COL1, MYH6, and CD31 (Abcam).

Gross examination and histological sections were analyzed by two independent pathologists in a blinded fashion. Interstitial inflammation refers to the presence of aggregates of leukocytes in the interstitium. Fibrosis analysis was done with the Image J program, by thresholding the acquired pictures, and then creating selections of the fibrotic areas. Two sections and two cell fields were analyzed in each condition in animals and in cultures, respectively. Thirteen sections were analyzed for the corresponding 13 patients.

Gene quantifications

Total RNA was extracted from CFs by the use of trizol (ThermoFisher Scientific) and chloroform. RNA was precipitated with isopropanol and then purified with ethanol 75%, and purity and concentration were determined by measuring the absorbance at 260 nm with the nanodrop spectrophotometer 2000 (ThermoFisher Scientific). Complementary DNA (cDNA) was synthesized by using random primers ($250\,ng\cdot\mu L^{-1}$), dNTP ($10\,mmol.L^{-1}$) and the superscript II reverse transcriptase kit (ThermoFisher Scientific).

Quantitative real-time polymerase chain reaction (PCR) was conducted by using the 7500 real-time PCR system and the Sybr green PCR master mix (ThermoFisher Scientific). Melting curves were performed at the end of the amplification to confirm the specificity of the amplified PCR products. In addition, ''no reverse transcriptase'' control reactions were done by omitting the reverse transcriptase to confirm the absence of contaminating genomic DNA. *GAPDH* was used as a housekeeping gene, and quantifications were conducted by using the $2^{\Delta\Delta Ct}$ method.

The primers (Eurogentec, Seraing, Belgium) used were as follows: *PCNA* F: 5′-GCAACTTGGAATCCCAGAACA-3′ and R: 5′-CCCGGCATATACGTGCAAAT-3′; *KI67* F: 5′-ATTTCAGTTCCGCCAATCC-3′ and R: 5′-GGCTTCC GTCTTCATACCTAAA-3′; *CCND1* F: 5′-AGATGAAGG AGACCATTCC-3′ and R: 5′-TTCAATCTGTTCCTGGCA G-3′; α-*SMA* (rat) F: 5′-ATGGCTCCGGGCTCTGTA A-3′ and R: 5′-ACAGCCCTGGGAGCATCA-3′; α-*SMA* (human) 5′-CCTGACTGAGCGTGGCTATT-3′ and R: 5′-GATGAAGGATGGCTGGAACA-3′; COL1 (rat) F: 5′-CTGGCGCAAGAGGCGAGAGA-3′ and R: 5′-AGCTCCGGGGGCACCAGTAT-3′; *COL1* (human) F: 5′-ACGAAGACATCCCACCAATC-3′ and R: 5′-ATGG TACCTGAGGCCGTTC-3′; *COL3* F: 5′-GTGGTAGCCC TGGTGAGA-3′ and R: 5′-GGGGGTCCTGGGTTAC-3′; *FN1* (rat) F: 5′-CGCCGAGCATTCTGCCGGAA-3′ and R: 5′-TCGGAAACCGTGGATTGCTGGC-3′; *FN1* (human) F: 5′-CGGTGGCTGTCAGTCAAAG-3′ and R: 5′-AAACCTC GGCTTCCTCCATAA-3′; *VIM* F: 5′-ATGAAAGTGTGGC TGCCAAGAAC-3′ and R: 5′-GTGACTGCACCTGTCTC CGGTA-3′; *SMEMB* F: 5′-GAAGCAGAAATCCTCCAG TTG-3′ and R: 5′-CGAGACGACCTACTCTTCG-3′; *Trpc3* (rat) F: 5′-GAGATCTGGAATCGGTGGAA-3′ and R: 5′-AAAAGCTGCTGTTGGCAGTT-3′; *TRPC3* (human) F: 5′-GGAAGGACTGTAAAGGACA-3′ and R: 5′-CACAACGG AAGTCACTTCA-3′; *CASP3* F: 5′-CAAGTCGATGGAC TCTGGAA-3′ and R: 5′-GTACCATTGCGAGCTGACAT-3′; *BCL2* F: 5′-CATGCGACCTCTGTTTGA-3′ and R: 5′-GTTTCATGGTCCATCCTTG-3′; *GAPDH* (rat) F: 5′-GGC TCTCTGCTCCTCCCTGTTCTA-3′ and R: 5′-GCCAAAT CCGTTCACACCGACCT-3′; *GAPDH* (human) F: 5′-TCCA TGACAACTTTGGTATCG-3′ and R: 5′-TGTAGCCAAA TTCGTTGTCA-3′.

Statistical analysis

All quantitative data are reported as mean ± SEM. Statistical analysis was performed with the SigmaPlot (v11.0) software. Normal distribution of the values was checked by the Shapiro-Wilk test. When normal distribution was met, one-way analysis of variance (ANOVA) tests were performed for multiple comparisons of values and *post hoc* Holm-Sidak tests were performed to identify which group differences accounted for significant overall ANOVA results. When normal distribution was not met, Kruskal-Wallis one-way ANOVA on ranks tests were performed, followed by Mann-Whitney U tests. Two-way ANOVA tests were performed followed by *post hoc* Holm-Sidak tests when two different independent variables with a single continuous response variable were present. Pearson correlation coefficient was used to measure the strength of the relationship between the variables when mentioned. All values with $p < 0.05$ were considered significant.

Acknowledgments

This work was supported by the Research Council of the Saint Joseph University, Faculty of Medicine and in part by the NIH Intramural Research Program (project Z01-ES-101684 to L.B. and J.A.). The authors are very thankful to Pr Nancy Rusch at the University of Arkansas for Medical Sciences for providing them with the TRPC3$^{-/-}$ mice.

Author Disclosure Statement

The authors declare that there are no conflicts of interest.

References

1. Braitsch CM, Kanisicak O, van Berlo JH, Molkentin JD, and Yutzey KE. Differential expression of embryonic epicardial progenitor markers and localization of cardiac fibrosis in adult ischemic injury and hypertensive heart disease. *J Mol Cell Cardiol* 65: 108–119, 2013.
2. Cassidy A, Mukamal KJ, Liu L, Franz M, Eliassen AH, and Rimm EB. High anthocyanin intake is associated with a reduced risk of myocardial infarction in young and middle-aged women. *Circulation* 127: 188–196, 2013.
3. Chacar S, Itani T, Hajal J, Saliba Y, Louka N, Faivre JF, Maroun R, and Fares N. The impact of long-term intake of phenolic compounds-rich grape pomace on rat gut microbiota. *J Food Sci* 83: 246–251, 2018.
4. Chen JB, Tao R, Sun HY, Tse HF, Lau CP, and Li GR. Multiple Ca^{2+} signaling pathways regulate intracellular Ca^{2+} activity in human cardiac fibroblasts. *J Cell Physiol* 223: 68–75, 2010.
5. D'Archivio M, Santangelo C, Scazzocchio B, Varì R, Filesi C, Masella R, and Giovannini C. Modulatory effects of polyphenols on apoptosis induction: relevance for cancer prevention. *Int J Mol Sci* 9: 213–228, 2008.
6. Davis J, Burr AR, Davis GF, Birnbaumer L, and Molkentin JD. A TRPC6-dependent pathway for myofibroblast transdifferentiation and wound healing in vivo. *Dev Cell* 23: 705–715, 2012.
7. Davis J and Molkentin JD. Myofibroblasts: trust your heart and let fate decide. *J Mol Cell Cardiol* 70: 9–18, 2014.
8. Del Rio D, Rodriguez-Mateos A, Spencer JP, Tognolini M, Borges G, and Crozier A. Dietary (poly)phenolics in human health: structures, bioavailability, and evidence of protective effects against chronic diseases. *Antioxid Redox Signal* 18: 1818–1892, 2013.
9. Dietrich A, Mederos y Schnitzler M, Gollasch M, Gross V, Storch U, Dubrovska G, Obst M, Yildirim E, Salanova B, Kalwa H, Essin K, Pinkenburg O, Luft FC, Gudermann T, and Birnbaumer L. Increased vascular smooth muscle contractility in TRPC6$^{-/-}$ mice. *Mol Cell Biol* 25: 6980–6989, 2005.
10. Dobrydneva Y, Williams RL, and Blackmore PF. Diethylstilbestrol and other nonsteroidal estrogens: novel class of store-operated calcium channel modulators. *J Cardiovasc Pharmacol* 55: 522–530, 2010.
11. Driesen RB, Nagaraju CK, Abi-Char J, Coenen T, Lijnen PJ, Fagard RH, Sipido KR, and Petrov VV. Reversible and irreversible differentiation of cardiac fibroblasts. *Cardiovasc Res* 101: 411–422, 2014.
12. Estruch R, Ros E, Salas-Salvado J, Covas MI, Corella D, Aros F, Gomez-Gracia E, Ruiz-Gutierrez V, Fiol M, Lapetra J, Lamuela-Raventos RM, Serra-Majem L, Pinto X, Basora J, Munoz MA, Sorli JV, Martinez JA, and Martinez-Gonzalez MA. Retraction and republication: primary

prevention of cardiovascular disease with a mediterranean diet. N Engl J Med 2013;368: 1279–90. *N Engl J Med* 378: 2441–2442, 2018.
13. Feng S, Li H, Tai Y, Huang J, Su Y, Abramowitz J, Zhu MX, Birnbaumer L, and Wang Y. Canonical transient receptor potential 3 channels regulate mitochondrial calcium uptake. *Proc Natl Acad Sci U S A* 110: 11011–11016, 2013.
14. Fujii T, Onohara N, Maruyama Y, Tanabe S, Kobayashi H, Fukutomi M, Nagamatsu Y, Nishihara N, Inoue R, Sumimoto H, Shibasaki F, Nagao T, Nishida M, and Kurose H. Galpha12/13-mediated production of reactive oxygen species is critical for angiotensin receptor-induced NFAT activation in cardiac fibroblasts. *J Biol Chem* 280: 23041–23047, 2005.
15. Goszcz K, Duthie GG, Stewart D, Leslie SJ, and Megson IL. Bioactive polyphenols and cardiovascular disease: chemical antagonists, pharmacological agents or xenobiotics that drive an adaptive response? *Br J Pharmacol* 174: 1209–1225, 2017.
16. Hartmann J, Dragicevic E, Adelsberger H, Henning HA, Sumser M, Abramowitz J, Blum R, Dietrich A, Freichel M, Flockerzi V, Birnbaumer L, and Konnerth A. TRPC3 channels are required for synaptic transmission and motor coordination. *Neuron* 59: 392–398, 2008.
17. Haudek SB, Xia Y, Huebener P, Lee JM, Carlson S, Crawford JR, Pilling D, Gomer RH, Trial J, Frangogiannis NG, and Entman ML. Bone marrow-derived fibroblast precursors mediate ischemic cardiomyopathy in mice. *Proc Natl Acad Sci U S A* 103: 18284–18289, 2006.
18. He X, Li S, Liu B, Susperreguy S, Formoso K, Yao J, Kang J, Shi A, Birnbaumer L, and Liao Y. Major contribution of the 3/6/7 class of TRPC channels to myocardial ischemia/reperfusion and cellular hypoxia/reoxygenation injuries. *Proc Natl Acad Sci U S A* 114: E4582–E4591, 2017.
19. Huang JH, He GW, Xue HM, Yao XQ, Liu XC, Underwood MJ, and Yang Q. TRPC3 channel contributes to nitric oxide release: significance during normoxia and hypoxia-reoxygenation. *Cardiovasc Res* 91: 472–482, 2011.
20. Kanisicak O, Khalil H, Ivey MJ, Karch J, Maliken BD, Correll RN, Brody MJ, J Lin SC, Aronow BJ, Tallquist MD, and Molkentin JD. Genetic lineage tracing defines myofibroblast origin and function in the injured heart. *Nat Commun* 7: 12260, 2016.
21. Karamać M. Chelation of Cu(II), Zn(II), and Fe(II) by tannin constituents of selected edible nuts. *Int J Mol Sci* 10: 5485–5497, 2009.
22. Kazakov A, Hall R, Jagoda P, Bachelier K, Müller-Best P, Semenov A, Lammert F, Böhm M, and Laufs U. Inhibition of endothelial nitric oxide synthase induces and enhances myocardial fibrosis. *Cardiovasc Res* 100: 211–221, 2013.
23. Kitajima N, Numaga-Tomita T, Watanabe M, Kuroda T, Nishimura A, Miyano K, Yasuda S, Kuwahara K, Sato Y, Ide T, Birnbaumer L, Sumimoto H, Mori Y, and Nishida M. TRPC3 positively regulates reactive oxygen species driving maladaptive cardiac remodeling. *Sci Rep* 6: 37001, 2016.
24. Kiyonaka S, Kato K, Nishida M, Mio K, Numaga T, Sawaguchi Y, Yoshida T, Wakamori M, Mori E, Numata T, Ishii M, Takemoto H, Ojida A, Watanabe K, Uemura A, Kurose H, Morii T, Kobayashi T, Sato Y, Sato C, Hamachi I, and Mori Y. Selective and direct inhibition of TRPC3 channels underlies biological activities of a pyrazole compound. *Proc Natl Acad Sci U S A* 106: 5400–5405, 2009.
25. Kopp RF, Leech CA, and Roe MW. Resveratrol interferes with Fura-2 intracellular calcium measurements. *J Fluoresc* 24: 279–284, 2014.
26. Kramann R, Schneider RK, DiRocco DP, Machado F, Fleig S, Bondzie PA, Henderson JM, Ebert BL, and Humphreys BD. Perivascular Gli1^{+} progenitors are key contributors to injury-induced organ fibrosis. *Cell Stem Cell* 16: 51–66, 2015.
27. Kuwahara K, Wang Y, McAnally J, Richardson JA, Bassel-Duby R, Hill JA, and Olson EN. TRPC6 fulfills a calcineurin signaling circuit during pathologic cardiac remodeling. *J Clin Invest* 116: 3114–3126, 2006.
28. Lighthouse JK and Small EM. Transcriptional control of cardiac fibroblast plasticity. *J Mol Cell Cardiol* 91: 52–60, 2016.
29. Lin CM, Chang H, Wang BW, and Shyu KG. Suppressive effect of epigallocatechin-3-O-gallate on endoglin molecular regulation in myocardial fibrosis in vitro and in vivo. *J Cell Mol Med* 20: 2045–2055, 2016.
30. Lin Z, Murtaza I, Wang K, Jiao J, Gao J, and Li PF. miR-23a functions downstream of NFATc3 to regulate cardiac hypertrophy. *Proc Natl Acad Sci U S A* 106: 12103–12108, 2009.
31. Liu Y, Gao L, Guo S, Liu Y, Zhao X, Li R, Yan X, Li Y, Wang S, Niu X, Yao L, Zhang Y, Li L, and Yang H. Kaempferol alleviates angiotensin II-induced cardiac dysfunction and interstitial fibrosis in mice. *Cell Physiol Biochem* 43: 2253–2263, 2017.
32. Macian F. NFAT proteins: key regulators of T-cell development and function. *Nat Rev Immunol* 5: 472–484, 2005.
33. Martínez-González MÁ, Toledo E, Arós F, Fiol M, Corella D, Salas-Salvadó J, Ros E, Covas MI, Fernández-Crehuet J, Lapetra J, Muñoz MA, Fitó M, Serra-Majem L, Pintó X, Lamuela-Raventós RM, Sorlí JV, Babio N, Buil-Cosiales P, Ruiz-Gutierrez V, Estruch R, Alonso A, PREDIMED Investigators. Extravirgin olive oil consumption reduces risk of atrial fibrillation: the PREDIMED (Prevencion con Dieta Mediterranea) trial. *Circulation* 130: 18–26, 2014.
34. McMurray JJ, Packer M, Desai AS, Gong J, Lefkowitz MP, Rizkala AR, Rouleau JL, Shi VC, Solomon SD, Swedberg K, and Zile MR; PARADIGM-HF Investigators and Committees. Angiotensin-neprilysin inhibition versus enalapril in heart failure. *N Engl J Med* 371: 993–1004, 2014.
35. Moore-Morris T, Cattaneo P, Guimarães-Camboa N, Bogomolovas J, Cedenilla M, Banerjee I, Ricote M, Kisseleva T, Zhang L, Gu Y, Dalton ND, Peterson KL, Chen J, Pucéat M, and Evans SM. Infarct fibroblasts do not derive from bone marrow lineages. *Circ Res* 122: 583–590, 2018.
36. Moore-Morris T, Guimarães-Camboa N, Banerjee I, Zambon AC, Kisseleva T, Velayoudon A, Stallcup WB, Gu Y, Dalton ND, Cedenilla M, Gomez-Amaro R, Zhou B, Brenner DA, Peterson KL, Chen J, and Evans SM. Resident fibroblast lineages mediate pressure overload-induced cardiac fibrosis. *J Clin Invest* 124: 2921–2934, 2014.
37. Nishida M, Onohara N, Sato Y, Suda R, Ogushi M, Tanabe S, Inoue R, Mori Y, and Kurose H. Galpha12/13-mediated up-regulation of TRPC6 negatively regulates endothelin-1-induced cardiac myofibroblast formation and collagen synthesis through nuclear factor of activated T cells activation. *J Biol Chem* 282: 23117–23128, 2007.
38. Noad RL, Rooney C, McCall D, Young IS, McCance D, McKinley MC, Woodside JV, and McKeown PP. Beneficial effect of a polyphenol-rich diet on cardiovascular risk: a randomised control trial. *Heart* 102: 1371–1379, 2016.
39. Numaga-Tomita T, Kitajima N, Kuroda T, Nishimura A, Miyano K, Yasuda S, Kuwahara K, Sato Y, Ide T,

Birnbaumer L, Sumimoto H, Mori Y, and Nishida M. TRPC3-GEF-H1 axis mediates pressure overload-induced cardiac fibrosis. *Sci Rep* 6: 39383, 2016.
40. Numaga-Tomita T, Oda S, Shimauchi T, Nishimura A, Mangmool S, and Nishida M. TRPC3 channels in cardiac fibrosis. *Front Cardiovasc Med* 4: 56, 2017.
41. Olson ER, Naugle JE, Zhang X, Bomser JA, and Meszaros JG. Inhibition of cardiac fibroblast proliferation and myofibroblast differentiation by resveratrol. *Am J Physiol Heart Circ Physiol* 288: H1131–H1138, 2005.
42. Onohara N, Nishida M, Inoue R, Kobayashi H, Sumimoto H, Sato Y, Mori Y, Nagao T, and Kurose H. TRPC3 and TRPC6 are essential for angiotensin II-induced cardiac hypertrophy. *EMBO J* 25: 5305–5316, 2006.
43. Orr AL, Vargas L, Turk CN, Baaten JE, Matzen JT, Dardov VJ, Attle SJ, Li J, Quackenbush DC, Goncalves RL, Perevoshchikova IV, Petrassi HM, Meeusen SL, Ainscow EK, and Brand MD. Suppressors of superoxide production from mitochondrial complex III. *Nat Chem Biol* 11: 834–836, 2015.
44. Park HW, Kim JY, Choi SK, Lee YH, Zeng W, Kim KH, Muallem S, and Lee MG. Serine–threonine kinase with-no-lysine 4 (WNK4) controls blood pressure via transient receptor potential canonical 3 (TRPC3) in the vasculature. *Proc Natl Acad Sci U S A* 108: 10750–10755, 2011.
45. Ponzo V, Soldati L, and Bo S. Resveratrol: a supplementation for men or for mice? *J Transl Med* 12: 158, 2014.
46. Potenza MA, Marasciulo FL, Tarquinio M, Tiravanti E, Colantuono G, Federici A, Kim JA, Quon MJ, and Montagnani M. EGCG, a green tea polyphenol, improves endothelial function and insulin sensitivity, reduces blood pressure, and protects against myocardial I/R injury in SHR. *Am J Physiol Endocrinol Metab* 292: E1378–E1387, 2007.
47. Prabhu SD and Frangogiannis NG. The biological basis for cardiac repair after myocardial infarction: from inflammation to fibrosis. *Circ Res* 119: 91–112, 2016.
48. Robich MP, Osipov RM, Nezafat R, Feng J, Clements RT, Bianchi C, Boodhwani M, Coady MA, Laham RJ, and Sellke FW. Resveratrol improves myocardial perfusion in a swine model of hypercholesterolemia and chronic myocardial ischemia. *Circulation* 122: S142–S149, 2010.
49. Rose RA, Hatano N, Ohya S, Imaizumi Y, and Giles WR. C-type natriuretic peptide activates a non-selective cation current in acutely isolated rat cardiac fibroblasts via natriuretic peptide C receptor-mediated signalling. *J Physiol* 580: 255–274, 2007.
50. Ruiz-Villalba A, Simón AM, Pogontke C, Castillo MI, Abizanda G, Pelacho B, Sánchez-Domínguez R, Segovia JC, Prósper F, and Pérez-Pomares JM. Interacting resident epicardium-derived fibroblasts and recruited bone marrow cells form myocardial infarction scar. *J Am Coll Cardiol* 65: 2057–2066, 2015.
51. Sahebkar A, Serban C, Ursoniu S, Wong ND, Muntner P, Graham IM, Mikhailidis DP, Rizzo M, Rysz J, Sperling LS, Lip GY, and Banach M; Lipid and Blood Pressure Meta-analysis Collaboration Group. Lack of efficacy of resveratrol on C-reactive protein and selected cardiovascular risk factors—results from a systematic review and meta-analysis of randomized controlled trials. *Int J Cardiol* 189: 47–55, 2015.
52. Saliba Y, Karam R, Smayra V, Aftimos G, Abramowitz J, Birnbaumer L, and Farès N. Evidence of a role for fibroblast transient receptor potential canonical 3 Ca^{2+} channel in renal fibrosis. *J Am Soc Nephrol* 26: 1855–1876, 2015.
53. Santiago JJ, Dangerfield AL, Rattan SG, Bathe KL, Cunnington RH, Raizman JE, Bedosky KM, Freed DH, Kardami E, and Dixon IM. Cardiac fibroblast to myofibroblast differentiation in vivo and in vitro: expression of focal adhesion components in neonatal and adult rat ventricular myofibroblasts. *Dev Dyn* 239: 1573–1584, 2010.
54. Scalbert A and Williamson G. Dietary intake and bioavailability of polyphenols. *J Nutr* 130: 2073S–2085S, 2000.
55. Schleifer H, Doleschal B, Lichtenegger M, Oppenrieder R, Derler I, Frischauf I, Glasnov TN, Kappe CO, Romanin C, and Groschner K. Novel pyrazole compounds for pharmacological discrimination between receptor-operated and store-operated Ca(2+) entry pathways. *Br J Pharmacol* 167: 1712–1722, 2012.
56. Schulz E, Wenzel P, Münzel T, and Daiber A. Mitochondrial redox signaling: interaction of mitochondrial reactive oxygen species with other sources of oxidative stress. *Antioxid Redox Signal* 20: 308–324, 2014.
57. Senadheera S, Kim Y, Grayson TH, Toemoe S, Kochukov MY, Abramowitz J, Housley GD, Bertrand RL, Chadha PS, Bertrand PP, Murphy TV, Tare M, Birnbaumer L, Marrelli SP, and Sandow SL. Transient receptor potential canonical type 3 channels facilitate endothelium-derived hyperpolarization-mediated resistance artery vasodilator activity. *Cardiovasc Res* 95: 439–447, 2012.
58. Seo K, Rainer PP, Shalkey Hahn V, Lee DI, Jo SH, Andersen A, Liu T, Xu X, Willette RN, Lepore JJ, Marino JP, Jr., Birnbaumer L, Schnackenberg CG, and Kass DA. Combined TRPC3 and TRPC6 blockade by selective small-molecule or genetic deletion inhibits pathological cardiac hypertrophy. *Proc Natl Acad Sci U S A* 111: 1551–1556, 2014.
59. Singh A, Hildebrand ME, Garcia E, and Snutch TP. The transient receptor potential channel antagonist SKF96365 is a potent blocker of low-voltage-activated T-type calcium channels. *Br J Pharmacol* 160: 1464–1475, 2010.
60. Singh CK, Liu X, and Ahmad N. Resveratrol, in its natural combination in whole grape, for health promotion and disease management. *Ann N Y Acad Sci* 1348: 150–160, 2015.
61. Spinale FG and Zile MR. Integrating the myocardial matrix into heart failure recognition and management. *Circ Res* 113: 725–738, 2013.
62. Thandapilly SJ, Louis XL, Behbahani J, Movahed A, Yu L, Fandrich R, Zhang S, Kardami E, Anderson HD, and Netticadan T. Reduced hemodynamic load aids low-dose resveratrol in reversing cardiovascular defects in hypertensive rats. *Hypertens Res* 36: 866–872, 2013.
63. Thandapilly SJ, Wojciechowski P, Behbahani J, Louis XL, Yu L, Juric D, Kopilas MA, Anderson HD, and Netticadan T. Resveratrol prevents the development of pathological cardiac hypertrophy and contractile dysfunction in the SHR without lowering blood pressure. *Am J Hypertens* 23: 192–196, 2010.
64. Tomida T, Hirose K, Takizawa A, Shibasaki F, and Iino M. NFAT functions as a working memory of Ca^{2+} signals in decoding Ca2+ oscillation. *EMBO J* 22: 3825–3832, 2003.
65. Travers JG, Kamal FA, Robbins J, Yutzey KE, and Blaxall BC. Cardiac fibrosis: the fibroblast awakens. *Circ Res* 118: 1021–1040, 2016.
66. Tresserra-Rimbau A, Rimm EB, Medina-Remón A, Martínez-González MA, López-Sabater MC, Covas MI, Corella D, Salas-Salvadó J, Gómez-Gracia E, Lapetra J, Arós F, Fiol M, Ros E, Serra-Majem L, Pintó X, Muñoz MA, Gea A, Ruiz-Gutiérrez V, Estruch R, and Lamuela-Raventós RM; PREDIMED Study Investigators. Polyphenol intake and mortality risk: a re-analysis of the PREDIMED trial. *BMC Med* 12: 77, 2014.

67. van Amerongen MJ, Bou-Gharios G, Popa E, van Ark J, Petersen AH, van Dam GM, van Luyn MJ, and Harmsen MC. Bone marrow-derived myofibroblasts contribute functionally to scar formation after myocardial infarction. *J Pathol* 214: 377–386, 2008.
68. Vennekens R. Emerging concepts for the role of TRP channels in the cardiovascular system. *J Physiol* 589: 1527–1534, 2011.
69. Visioli F. The resveratrol fiasco. *Pharmacol Res* 90: 87, 2014.
70. Wang B, Xiong S, Lin S, Xia W, Li Q, Zhao Z, Wei X, Lu Z, Wei X, Gao P, Liu D, and Zhu Z. Enhanced mitochondrial transient receptor potential channel, canonical type 3-mediated calcium handling in the vasculature from hypertensive rats. *J Am Heart Assoc* 6: e005812, 2017.
71. Yue Z, Xie J, Yu AS, Stock J, Du J, and Yue L. Role of TRP channels in the cardiovascular system. *Am J Physiol Heart Circ Physiol* 308: H157–H182, 2015.
72. Zeisberg EM, Tarnavski O, Zeisberg M, Dorfman AL, McMullen JR, Gustafsson E, Chandraker A, Yuan X, Pu WT, Roberts AB, Neilson EG, Sayegh MH, Izumo S, and Kalluri R. Endothelial-to-mesenchymal transition contributes to cardiac fibrosis. *Nat Med* 13: 952–961, 2007.
73. Zhou B, Honor LB, He H, Ma Q, Oh JH, Butterfield C, Lin RZ, Melero-Martin JM, Dolmatova E, Duffy HS, Gise Av, Zhou P, Hu YW, Wang G, Zhang B, Wang L, Hall JL, Moses MA, McGowan FX, and Pu WT. Adult mouse epicardium modulates myocardial injury by secreting paracrine factors. *J Clin Invest* 121: 1894–1904, 2011.
74. Zitt C, Strauss B, Schwarz EC, Spaeth N, Rast G, Hatzelmann A, and Hoth M. Potent inhibition of Ca^{2+} release-activated Ca^{2+} channels and T-lymphocyte activation by the pyrazole derivative BTP2. *J Biol Chem* 279: 12427–12437, 2004.

Address correspondence to:
Prof. Nassim Farès
Laboratoire de Physiologie et Physiopathologie
Pôle Technologie Santé
Faculté de Médecine
Université Saint Joseph
Damascus Street
BP 11-5076 - Riad El Solh
Beirut 1107 2180
Lebanon

E-mail: nassim.fares@usj.edu.lb

Date of first submission to ARS Central, March 14, 2018; date of final revised submission, September 26, 2018; date of acceptance, October 8, 2018.

Abbreviations Used

α-SMA = alpha smooth muscle actin
8-OHDG = 8-hydroxy-2′-deoxyguanosine
AngII = angiotensin II
ANOVA = analysis of variance
BCL2 = B cell lymphoma 2
BNP = brain natriuretic peptide
BSA = bovine serum albumin
CASP3 = caspase 3
CCND1 = cyclin D1
CF = cardiac fibroblast
COL1 = collagen 1
COL3 = collagen 3
COX4 = cytochrome c oxidase subunit 4
CPA = cyclopiazonic acid
CRP = C-reactive protein
CsA = cyclosporine A
DAG = diacylglycerol
DAPI = 4′,6-diamidino-2-phenylindole
DCF = 2′,7′-dichlorofluorescein
DMEM = Dulbecco's modified Eagle's medium
DMSO = dimethylsulfoxide
ECM = extracellular matrix
EF = ejection fraction
EGTA = ethylene glycol tetraacetic acid
ELISA = enzyme-linked immunosorbent assay
eNOS = endothelial nitric oxide synthase
FBS = fetal bovine serum
FN1 = fibronectin 1
FS = fractional shortening
GAPDH = glyceraldehyde-3-phosphate dehydrogenase
HPLC = high performance liquid chromatography
H_2DCF-DA = 2′,7′-dichlorodihydrofluorescein diacetate
IL1 = interleukin 1
IVSTd = end-diastolic interventricular septal wall thickness
L-NAME = N(ω)-nitro-L-arginine methyl ester
LVIDd = left ventricular end-diastolic internal dimension
LVPWd = end-diastolic left ventricular posterior wall thickness
MF = myocardial fibrosis
MTT = 3-(4,5-dimethylthiazol-2-yl)-2,5-diphenyltetrazolium bromide
NFATc3 = nuclear factor of activated T cells c3
Nox = NADPH oxidase
OAG = 1-oleoyl-2-acetyl-*sn*-glycerol
PBS = phosphate-buffered saline
PCNA = proliferating cell nuclear antigen
PCR = polymerase chain reaction
PDGFRα = platelet-derived growth factor receptor alpha
P.E. = extract of grape pomace polyphenol
p-eNOS = phospho-eNOS
Pyr10 = N-[4-[3,5-Bis(trifluoromethyl)-1H-pyrazol-1-yl]phenyl]-4-methyl-benzenesulfonamide
ROCE = receptor-operated Ca^{2+} entry
ROS = reactive oxygen species
SEM = standard error of the mean
SMEMB = embryonic smooth muscle myosin heavy chain
SOCE = store-operated Ca^{2+}ium entry
TCF21 = transcription factor 21
TGF-β1 = transforming growth factor beta 1
TNF-α = tumor necrosis factor alpha
TnT = troponin T
TRPC3 = transient receptor potential canonical 3
VIM = vimentin
WT = wild-type